A proteomic map of B cell activation and its shaping by mTORC1, MYC and iron

Olivia James[1,2,*], Linda V. Sinclair[1,*], Nadia Lefter[1], Fiamma Salerno[3], Alejandro Brenes[4] and Andrew J.M. Howden[1]

[1] Division of Cell Signalling and Immunology, School of Life Sciences, University of Dundee

[2] Current address: GSK, Gunnels Wood Road, Stevenage

[3] Department of Immunology, Leiden University Medical Center, Leiden, Netherlands

[4] Centre for Inflammation Research, Institute for Regeneration and Repair, University of Edinburgh

* These authors contributed equally

Corresponding author: a.howden@dundee.ac.uk

Summary

Using high resolution quantitative mass spectrometry, we have explored how immune activation and the metabolic checkpoint kinase mTORC1 (mammalian target of rapamycin complex 1) regulate the proteome of B lymphocytes. B cell activation via the B cell receptor, CD40 and the IL-4 receptor induced considerable re-modelling of the B cell protein landscape, with a 5-fold increase in total cellular protein mass within 24 hours of activation. Analysis of copy numbers per cell of >7,500 proteins revealed increases in the metabolic machinery that supports B cell activation and nutrient and amino acid transporters that fuel B cell biosynthetic capacity. We reveal that mTORC1 controls activation-induced cell growth and B cell proteome remodelling and inhibiting mTORC1 impairs the expression of amino acid transporters that fuel B cell protein production. We also show that mTORC1 activity regulates the expression of the transcription factor MYC and the transferrin receptor CD71. Blocking MYC activity phenocopied mTORC1 inhibition in many ways including impaired

CD71 expression, while limiting iron availability during B cell activation impaired B cell growth and protein synthesis. This work provides a detailed map of naïve and immune activated B cell proteomes and a greater understanding of the cellular machinery that direct B cell phenotypes. This work also provides new insights into the role of mTORC1, MYC and iron in regulating activation-induced proteome remodelling and protein production in B cells.

Introduction

B lymphocytes (B cells) are a key component of the adaptive immune system, producing antibodies for targeting bacteria and viruses, secreting pro- and anti-inflammatory cytokines and presenting antigen to T cells. B cell function is critical for maintaining health and as such B cell dysfunction is linked to a broad spectrum of diseases including autoimmunity and immunodeficiency, diseases of the central nervous system and B cell malignancies. B cells sense and respond to their environment using the B cell receptor (BCR) and a range of other cell surface receptors including CD40, which binds to CD40 ligand (CD40L) expressed on the surface of T cells, the pattern recognition Toll-Like Receptors including TLR4, which is triggered by lipopolysaccharide, and cytokine receptors including interleukin 4 receptor (IL4R) and interleukin 21 receptor (IL21R). Immune activation of B cells triggers transcriptional re-programming and elicits changes in metabolism and protein production that in turn drive proliferative expansion and B cell differentiation. Effective B cell activation will give rise to populations of short and long-lived antibody producing plasma cells as well as memory B cells. Thus, activated B cells need to ramp up metabolism and protein production appropriately to sustain these diverse fates.

A central metabolic regulator that controls protein synthesis in mammalian cells is the nutrient sensing serine/threonine protein kinase complex mTORC1 [1]. Various studies have outlined the importance of mTORC1 in B cell growth and differentiation, placing the nutrient-regulated kinase as a critical regulator of B cell function. mTORC1 is important in B cell class switching, somatic hypermutation, memory B cell formation and the unfolded protein

response [2–6]. However, the mechanistic details of how mTORC1 regulates B cell activation, metabolism and protein synthesis are still to be fully mapped. Given the cell-type and cell-context specific impacts of mTORC1, a detailed analysis of the role of mTORC1 in B cell activation is needed if we are to fully understand its importance during immune challenge.

Quantitative proteomics is a valuable tool to understand immune cell phenotypes and cellular responses to stimulation, stress and the modulation of critical signalling pathways[7–10]. A deep characterisation of the protein landscape of the cell may help to bridge the gap between transcriptional changes and metabolic readouts, providing quantitative data on the metabolic machinery and regulators that drive cell phenotypes and function. In this study we have used high sensitivity quantitative mass spectrometry to map the activated B cell proteome. We identify and quantify over 7500 proteins in naïve and activated B cells and provide estimates of absolute copy numbers per cell for each protein. We find that the naïve B cell increases its protein mass 5-fold within 24 hours of activation leading to over 5000 proteins increasing in abundance and a handful of proteins dropping in abundance including regulators of translation and cell cycle. We highlight the core processes and metabolic machinery that are regulated by B cell activation and demonstrate the critical role of the System L large neutral amino acid transporter SLC7A5 in B cell activation. We reveal that selectively blocking mTORC1 activity dramatically impacts activation-induced proteome remodelling and impairs B cell protein production. mTORC1 activity is required for the sustained expression of the transcription factor MYC and for the upregulation of amino acid transporters that fuel B cell protein production, including SLC7A5. mTORC1 also regulates the expression of the transferrin receptor CD71, which is critical for iron uptake in cells. Inhibiting MYC phenocopied many of the effects of mTORC1 inhibition including the reduced expression of CD71, while limiting iron availability during B cell activation impaired B cell growth and protein synthesis. Together this data provides a valuable resource for the immunology community. We provide new insight into how B cells respond to stimulation and modulate their core metabolic processes and machinery for fuelling protein synthesis,

shedding new light on the role of mTORC1, MYC and iron during B cell activation. Our proteomics data is freely available and easy to explore on the Immunological Proteome Resource[11] www.immpres.co.uk.

Results

Activation-induced proteome remodelling in B cells

To assess the intrinsic changes driven by B cell activation, high resolution quantitative mass spectrometry was used to characterise the proteomes of primary naïve and immune-activated B cells, identifying and quantifying >7500 proteins. 24hr stimulation of B cells with anti-IgM, anti-CD40 and IL-4 resulted in a considerable increase in B cell size as shown by flow cytometry (Fig 1a) and a 5-fold increase in total cellular protein mass (Fig 1b). Using the proteomic ruler [12] we estimated the copy numbers per cell of all proteins identified in naïve and activated B cells. Proteins were ranked according to their estimated copy number per cell and plotted against their cumulative contribution to total protein abundance, to evaluate which proteins dominate the protein mass of naïve and activated B cells (Fig 1c). In naïve B cells, the 7 most abundant proteins which contribute 50% of the total protein mass of the cell are largely histones and cytoskeleton molecules while in activated cells 147 proteins contribute 50% of the total protein mass and includes ribosomal proteins and translational machinery, revealing that immune activation remodels the core proteome of B cells to drive protein synthesis (Fig 1c). To explore this further we analysed the contribution of different cellular compartments to the overall protein mass of the cell. Ribosomal proteins made up ~3% of the total protein mass of naïve cells which increased to 9% following activation, while mitochondrial proteins rose from 11% to 16% (Fig 1d). Some components such as the nuclear envelope and plasma membrane, were present in higher copies following activation but when adjusted against the total cellular protein content, showed little change relative to the total proteome (Fig 1d).

To examine protein changes in more detail, differential expression analysis was performed and revealed that >5800 proteins were significantly increased in expression >1.5-fold and with a p value <0.05 in activated B cells as compared to naïve (Fig 1e). The full data set along with fold changes, p values and q values can be found in Supplementary File 1. Among those proteins increasing in abundance were activation receptors CD86, CD69 and CD44 (Supplementary File 1). 56 proteins were found exclusively in naïve B cells and not in activated B cells, suggesting that they may be degraded upon B cell stimulation. These proteins included molecules controlling B cell quiescence such as the transcription factor KLF2 [13–15] (Fig 1e). Only 50 proteins were significantly downregulated upon B cell activation. Among those proteins significantly downregulated upon B cell activation were negative regulators of key processes facilitating protein synthesis and proliferation such as the mRNA translational repressor PDCD4 [16,17] and the cell cycle inhibitor p27 (CDKN1B) (Fig 1e). The loss of p27 was accompanied by an increase in positive regulators of cell cycle such as cyclin-dependent kinases (CDK1-4), as well as A-type, B-type, and D-type cyclins (Fig 1f). Subunits of the EIF4F translational complex responsible for mRNA translation also showed an increase in abundance and corresponding the loss of PDCD4 (Fig 1g).

Considering that naïve B cells increased their total protein content 5-fold following 24h immune activation, we performed subsequent analysis on proteins increasing in expression >5-fold to capture changes out-with the overall scaling up of protein mass following activation. We performed GO term enrichment analysis on proteins changing more than 5-fold or present only in activated B cells and found that enriched pathways included ribosome biogenesis, protein folding, mitochondrial translation, and Golgi vesicle transport (Fig 1h). Among the proteins enriched in Golgi vesicle transport were components of the coat protein complex II (COPII) involved in anterograde transport, including SAR1B, Sec23p/Sec24p and the Sec13p/Sec31p heterodimers[18–21] (Fig 1i). These data suggest that at 24h hrs of stimulation, B cells already begin to switch on trafficking machinery to support high levels of protein export necessary for antibody secretion. There was also considerable modulation of

transcription factor expression upon B cell activation. Over 400 proteins with predicted transcription factor activity were identified within the data set (Fig 2a and Supplementary File 1). Most of these transcription factors increased in abundance in response to immune activation and some were only detected in activated cells including NFIL3, AHR and JUNB (Fig 2b). NFIL3 expression is regulated by IL4 and is critical for B cell class switching [22]. Other transcription factors were considerably upregulated upon activation, including IRF4 which increased from around 4,000 copies per cell in naïve B cells to over 200,000 copies per cell upon activation. EGR2, which controls antigen receptor induced proliferation in B cells [23], increased from around 200 copies in naïve cells to almost 70,000 copies upon activation. Some transcription factors increased by a much smaller scale including PAX5 (Supplementary File 1), which increased less than 2-fold and which has previously been shown to be important during B cell development [24,25]. A small number of transcription factors were downregulated upon activation or were exclusively found in naïve cells including ELK4, CXXC5 and KLF2 (Fig 2b).

Immune activation drives nutrient transporter expression and metabolic and mitochondrial remodelling

24-hour B cell activation was accompanied by a considerable increase in cell size and total protein content. This rapid increase in cell size is energetically demanding and would require increased uptake of nutrients to fuel anabolic processes. We next asked which nutrient transporters were expressed in response to B cell activation. Several solute carrier (SLC) molecules were upregulated upon activation including amino acid transporters SLC1A5, a glutamine transporter, and SLC7A5 which transports many essential amino acids including methionine, tryptophan and leucine [26,27] (Fig 3a). Expression of these transporters was extremely low in naïve B cells (Fig 3a). SLC7A5 is critical for antigen-driven T cell responses, T cell differentiation and effector function [28,29].To explore the importance of SLC7A5 in B cell activation we used splenocytes from VavCre x *Slc7a5*$^{fl/fl}$ mice [28]. In these mice, VavCre drives deletion of *Slc7a5* in early haematopoietic development. Splenocytes

from VavCre x *Slc7a5*$^{fl/fl}$ mice were activated using anti-IgM and anti-CD40. The SLC7A5 KO B cells were considerably smaller than cre negative controls after activation (Fig 3b). SLC7A5 KO B cells also showed reduced expression of CD98, the heavy chain chaperone which forms a heterodimer with many amino acid transporters, including SLC7A5 and SLC7A6 [30]. Additionally, SLC7A5 KO B cells had impaired expression of the transferrin receptor CD71 in response to immune activation. CD71 is essential for iron uptake which fuels multiple metabolic processes in B cells [31–33] (Fig 3b). Together this data highlights the important role of a single amino acid transporter in fuelling the increase in size and the upregulation of key proteins that fuel B cell immune activation.

We next wanted to understand in greater detail the metabolic shift in B cells that occurs upon activation [34]. Using estimates of protein copy per cell we mapped glycolytic enzymes and enzymes that drive the pentose-phosphate pathway and one carbon metabolism. Previous studies have questioned the importance of glycolysis in B cell activation, suggesting instead that activated B cells switch on oxidative phosphorylation and the tricarboxylic acid cycle (TCA cycle) but not glycolysis [35]. The proteomic data show that expression of the glycolytic machinery, including rate-limiting glucose and lactate transporters [36] as well as glycolytic enzymes are considerably upregulated upon B cell activation (Fig 3c). Indeed, the glucose and lactate transporters SLC2A1 and SLC16A1 were virtually undetectable in naïve cells but were found in tens of thousands of copies upon B cell activation (Fig 3c and Supplementary File 1). The cellular mass of enzymes involved in one-carbon metabolism increased 10-fold in response to B cell activation, suggesting changes in metabolic enzymes that are beyond just scaling with increased cell size (Fig 3c).

Activation induced mitochondrial re-modelling has been well documented in B cells [34,35,37,38]. Using Mitocarta [39], predicted mitochondrial proteins were annotated within our data set, revealing that total mitochondrial molecules increased approximately 6-fold upon B cell activation (Fig 3d). To explore changes in mitochondrial processes that were independent of

activation-induced mitochondrial scaling, we adjusted protein copy numbers by the total mitochondrial protein molecules to determine their relative contribution. This analysis revealed mitochondrial proteins and processes that didn't just follow the scaled increase in mitochondrial mass (Fig 3d). For example, mitochondrial ribosomes increased 3-fold when adjusted against total mitochondrial molecules, suggesting increased dedication towards mitochondrial protein synthesis in the activating cell. In contrast, molecules involved in oxidative phosphorylation showed a diverse expression pattern with some, including cytochrome C1 and F-type ATPase subunits, remaining at similar concentrations in naïve and activated B cells, suggesting a scaled increase in abundance (Fig 3d).

Having noted significant increases in amino acid, glucose and lactate transporter expression upon B cell activation (Fig 3a and c) we also found considerable upregulation of the transferrin receptor CD71 (TFRC) from around 3000 copies per cell in naïve B cells to approximately 0.5 million copies upon activation (Fig 3e). Using annotations of iron-regulated proteins [40] we examined the expression profile of iron-interacting proteins in naïve and activated B cells. We detected 151 iron-regulated proteins in our proteomics data. These included proteins involved in Fe-S cluster synthesis, histone modification (Jmjd family proteins, Kdm family proteins), DNA synthesis (Pol family proteins), and OXPHOS (Fig 2f and Supplementary File 1). To gain a clearer understanding of the cellular requirements for iron, we estimated the total iron-content of the naïve and activated B cells. We assumed that all iron interacting sites were fully occupied and used known values of iron atoms per protein (where possible). Where exact values were not known we used a deliberate underestimation of 1 iron atom for heme or iron ion interaction, and 2 iron atoms for Fe-S cluster interactions, as described by Teh et al [40]. Using the protein copy numbers from our data, these calculations showed that the iron demand, or requirement, in naïve T cells is approximately 5 million iron atoms per cell. The demand for iron is increased 7-fold to 35 million iron atoms per cell in activated B cells (Fig 2g). These increased requirements for iron, to drive DNA

synthesis, histone modifications and mitochondrial functions, are matched by the increased expression of CD71 (TFRC).

mTORC1 activity drives protein biosynthesis and the machinery for fuelling B cells

Given the central role that mTORC1 plays in regulating diverse cellular responses including lymphocyte growth and differentiation [2,5,41–44] we next wanted to explore how mTORC1 regulates the protein biosynthetic capacity of activating B cells and the impact of blocking mTORC1 activity on B cell proteome remodelling. To selectively block mTORC1 during B cell activation, cells were treated with rapamycin and mTORC1 activity monitored through the phosphorylation of ribosomal protein S6, a downstream target of active mTORC1 signalling. Blocking mTORC1 activity with rapamycin during B cell activation reduced S6 phosphorylation to levels similar to those observed in naïve B cells (Fig 4a). Rapamycin treated cells were significantly smaller in size and had approximately half the total cellular protein mass when compared to control activated cells (Fig 4b and 4c). Further, B cells activated with rapamycin exhibited a considerable reduction in rates of protein synthesis compared to untreated cells, as measured by the incorporation of an analogue of puromycin into elongating protein chains in the ribosome (Fig 4d). We sought to understand how the inhibition of mTORC1 was driving the reduction in rates of protein synthesis and consequent decrease in protein mass. Proteomic analysis of cells treated with rapamycin revealed that >4800 proteins had reduced abundance when mTORC1 activity was blocked, while only 40 proteins were found at increased levels (Fig 4e). GO term enrichment analysis revealed that mTORC1 inhibition had a profound effect on many of the processes highly upregulated by B cell activation, including ribosome biogenesis, protein folding and mitochondrial translation (Fig 4f). A closer examination revealed that ribosomal protein mass and mitochondrial protein mass were both significantly reduced in response to blocking mTORC1 (Fig 4g). Transcription factors were among some of the most rapamycin-sensitive proteins in B cells. IRF4, a critical regulator of B cell reprogramming during early activation [45] , was found at significantly lower levels in rapamycin treated cells (Fig 4h). IRF8 expression was also

significantly impaired when mTORC1 activity was blocked. IRF8 has previously been shown to be important during B cell development and B cell germinal centre responses [46–48], although the role of IRF8 during B cell activation remains unclear. Our proteomic data also revealed high expression of AHR exclusively in activated B cells, which was found at significantly reduced levels, along with the Aryl Hydrocarbon Receptor Nuclear Translocator (ARNT), by rapamycin treatment (Fig 4i). AHR deletion has been shown to impact B cell proliferation [49]. Interestingly, several cyclin dependent kinases were found at significantly reduced levels in response to mTORC1 inhibition, notably CDK1, which was found at over 120,000 copies per cell in activated B cells, but only 5,000 copies in B cells activated with rapamycin (Supplementary File 1). Together, this data suggests that blocking mTORC1 with rapamycin significantly impacts activation-induced proteome remodelling, reducing the abundance of key proteins involved in ribosomal and mitochondrial mass, transcriptional regulation, proliferation and cell cycle progression.

mTORC1 inhibition also caused reduced expression of solute carrier proteins (Fig 4j) including the glucose transporter SLC2A1, the lactate transporter SLC16A1 and the System L amino acid transporter SLC7A5 (Fig 4k). The transferrin receptor CD71 and the mitochondrial iron transporter ABCB7 were also significantly reduced in abundance in mTORC1 inhibited cells (Fig 4k). To explore the mTORC1 impact on amino acid transport further we interrogated the System L amino acid transport capacity of B cells using a sensitive, flow cytometry based assay [50]. Uptake of the fluorescent SLC7A5 substrate kynurenine was impaired in B cells activated in the presence of rapamycin, orthogonally validating our proteomics data showing reduced levels of SLC7A5 abundance (Fig 5a, 5b, 5c). Flow cytometry analysis also revealed reduced abundance of CD98 (Fig 5d, 5e) and the transferrin receptor CD71 (Fig 5f, 5g). We next assessed the expression of iron interacting proteins in response to mTORC1 inhibition (Fig 5h) and found that many were considerably reduced in abundance including dioxygenase enzymes ALKBH1-8, a selection of cytochromes, NDUF molecules that are critical for oxidative phosphorylation along with

components of the DNA replication fork complex (Fig 5h). Taken together, these data suggest that mTORC1 plays a crucial role in regulating nutrient uptake in B cells, including the regulation of iron transporters and iron interacting molecules.

mTORC1 regulates MYC expression in B cells

We questioned whether mTORC1 driven effects on nutrient transport in B cells could in part be explained by an impact on MYC abundance. MYC is a master regulator of cellular metabolism and growth and controls amino acid transporter expression in T cells[51]. MYC is challenging to identify by mass spectrometry, most likely due to its constant turnover. We therefore monitored MYC expression in response to mTORC1 inhibition using a MYC-GFP reporter mouse [52]. We found that MYC was upregulated upon B cell activation, but MYC expression was significantly reduced in rapamycin treated cells at 4 hours and 24 hours (Fig 5i and 5j), suggesting the mTORC1 activity is required for maximal MYC expression during B cell activation. Having revealed that mTORC1 activity impacts MYC expression in activating B cells we next sought to understand the consequence of directly blocking MYC activity on B cells. To block MYC at the point of activation, B cells were treated with a small molecule inhibitor of MYC, MYCi361, which inhibits the formation of MYC:MAX heterodimers and blocks the ability of MYC to bind DNA [53]. Mass spectrometry was used to evaluate the impact of MYC inhibition on the B cell protein landscape while flow cytometry of key surface markers was used for validation. B cells activated in the presence of MYCi361 were reduced in size compared to control cells, according to their forward scatter profile (Fig 6a) and total protein copies per cell was also reduced in response to MYC inhibition (Fig 6b). Over 2500 proteins showed reduced abundance when MYC activity was blocked (Fig 6c). Included in those proteins that were reduced in abundance were ribosomal proteins (Fig 6d). In activated B cells ribosomal proteins totalled over $1.5x10^8$ copies per cell while in MYC inhibitor treated cells this reduced to approximately $0.75x10^8$ copies (Fig 6d). Components of the DNA replication fork machinery were also considerably reduced in expression upon MYC

inhibition, in some cases more than 5-fold (Table 1). The impact of MYC inhibition on DNA replication proteins was strikingly similar when compared with rapamycin treated cells (Table 1), highlighting the overlap between mTORC1 and MYC regulated proteins in B cells. Using our proteomics data along with orthogonal validation by flow cytometry, we found that the homing receptor CD62L and the activation marker CD69 were not impacted by MYCi361 (Fig 6e-h), in agreement with observations in activating T cells with a MYC KO [51]. However, the transferrin receptor CD71 (TFRC) showed significantly reduced abundance in response to MYCi361 as measured by mass spectrometry along with cell surface staining and flow cytometry (Fig 6i and j). CD71 expression is dependent on MYC expression in CD8 T cells [54] and also in B cells [55]. In addition to reduced abundance of CD71, iron interacting proteins were among those down-regulated upon MYC inhibition (Fig 6k). Interestingly, aside from CD71, nutrient and amino acid transporters were largely unimpacted by MYC inhibition (Supplementary File 1).

Iron availability is essential for B cell growth and protein synthesis

Receptor mediated endocytosis through the transferrin receptor CD71 is the primary method by which lymphocytes take up iron from their extracellular environment. Mutations in CD71 are linked with impaired lymphocyte function and immunodeficiency[31] . Having found that CD71 expression is regulated by SLC7A5 transporter expression along with mTORC1 activity and MYC activity, we next tested whether iron availability regulates activation-induced B cell growth and protein synthesis. Using the iron chelator deferiprone (3-Hydroxy-1,2-dimethyl-4(1H)-pyridone) B cells were activated for 24 hours in iron depleting conditions and monitored by flow cytometry to assess cell size, activation and protein synthesis. Iron chelation impaired the increase in cell size seen upon B cell activation, with increasing concentrations of deferiprone corelating with decreased cell size (Fig 7a, 7b and 7c). However, B cells were still able to upregulate the activation marker CD69 in iron limiting conditions (Fig 7d and 7e). Protein synthesis was significantly increased in activated B cells when compared with IL4 maintained cells but dropped with increasing concentration of the

iron chelator (Fig 7f). Higher concentrations of deferiprone (100μM and 300μM) brought levels of protein synthesis down to levels seen in IL4 maintained cells. Together this data shows that iron availability is a critical regulator of activation-induced cell growth in B cells.

Discussion

In this work we have mapped the protein landscape of naïve B cells and their response to activation through the B cell receptor, CD40 and the IL4 receptor. Our data reveals the scale of proteome remodelling triggered by B cell activation and the dramatic reconfiguration of cellular compartments including mitochondria and ribosomes. This study aimed to identify the metabolic regulators of B cell activation and protein synthesis. One important biological insight was the identification of the repertoire of amino acid transporters that are expressed upon B cell activation. Deleting one of these transporters, SLC7A5 which transports methionine, tryptophan and leucine, was catastrophic for B cell activation. SLC7A5 has previously been shown to be important during B cell development, with SLC7A5 deletion mice showing reduced B1 B cell numbers [56] . We now reveal an important role for SLC7A5 during B cell activation. In a complementary study Cheung et al., (personal communication) reveal the importance of SLC7A5 during LPS-mediated B cell activation, with SLC7A5 KO B cells showing impaired activation and proliferation. Together our studies show the fundamental role of a single amino acid transporter in B cell activities.

To understand the metabolic regulation of B cells we examined the impact of blocking mTORC1 activity during B cell activation. While mTORC1 is firmly established as a key regulator of metabolism and protein synthesis[57,58] , the mechanisms by which it does this in different cell types is yet to be fully mapped. Inhibiting mTORC1 had a considerable impact on protein production during B cell activation, and cells activated in the presence of rapamycin had a reduction in total protein mass of approximately 50% compared to control

activated cells. We found that SLC7A5 expression was regulated by mTORC1, with rapamycin treated cells showing reduced abundance of SLC7A5 and reduced SLC7A5-mediated amino acid uptake. We also found that mTORC1 activity regulates the expression of the transferrin receptor CD71. mTORC1 also regulates the expression of transcription factors that direct B cell activation and differentiation including IRF's, AHR and MYC. In T cells, the transcription factor MYC is required for the expression of SLC7A5, along with a selection of other nutrient transporters including CD71[51]. Inhibiting MYC activity in B cells phenocopied many of the mTORC1 inhibition effects including a considerable impact on the cell's DNA replication machinery, ribosomal protein content and the abundance of CD71. Interestingly, while mTORC1 and MYC are considered master regulators of cellular metabolism, their inhibition did not completely block protein synthesis. Much of the B cell protein landscape is not regulated by mTORC1 or MYC and B cells still considerably increased their cellular protein content despite mTORC1 and MYC inhibition. This highlights that the regulatory pathways for protein synthesis and cell growth are complex. Additional hubs are likely to be important and the interplay between hubs or their combinatorial effects may modulate B cell activation and cell growth. In addition, the nutrient environment is likely to be a fundamental driver of B cell responses. Understanding how B cells respond to nutrient stress during activation and how this impacts mTORC1 and MYC driven pathways is an important next step.

Iron has been widely shown to be essential for immune cell function. In B cells, iron availability is required for proliferation and antibody responses[59,60]. Our findings show that mTORC1 activity, SLC7A5 expression and MYC activity all regulate CD71 expression during B cell activation. We questioned whether mTORC1 and MYC mediated proteome remodelling could in large part be attributed to iron availability. Indeed, chelating iron during B cell activation impaired B cell growth and protein synthesis. Our data points towards CD71 and iron availability being a key regulatory hub for B cell activation.

In conclusion, this study provides in-depth proteomic maps of naïve and activated B cells and the impact of modulating key signalling pathways during B cell activation. This data provides new insights into the control of protein synthesis and cell growth in B cells and the machinery that drive B cell activation and environmental sensing.

Methods

Mice

Male wildtype C57BL/6 mice (Charles Rivers) aged between 8 and 12 weeks were used for proteomics experiments and for validation experiments examining protein synthesis, amino acid uptake and marker expression. Myc-eGFP mice[52] were used to monitor MYC expression by flow cytometry. VavCre x *Slc7a5*$^{fl/fl}$ mice were generated and described previously [28]. All mice were maintained in the Biological Resource Unit at the University of Dundee using procedures approved by the University Ethical Review Committee and under the authorization of the UK Home Office Animals (Scientific Procedures) Act 1986.

Culturing B cells and cell sorting

All cells were cultured at 37 ˚C with 5 % CO_2 in RPMI 1640 containing glutamine (Invitrogen) and supplemented with 10 % FBS (Gibco), 50 μM β-mercaptoethanol (Sigma) and penicillin/streptomycin (Gibco). For proteomic experiments lymph nodes were extracted from mice, mashed in RPMI media before filtering through a 70 μm cell strainer. For generating a pure population of naïve B cells, lymphocytes were incubated with FC block and then stained with CD19 FITC, CD93 APC and DAPI. CD19+ and CD93- live cells were sorted using a Sony LE-MA900. Sorted cells were washed twice with HBSS and snap frozen in liquid nitrogen and stored at -80 °C until processing for mass spectrometry. For B cell activation, lymphocytes were suspended in RPMI at a final density of 1.5 million cells/ml and

activated for 24 hours in the presence of 10 μg/ml Anti-IgM (AffiniPure F(ab')$_2$ fragment goat anti-mouse), 10 μg/ml anti-CD40 (FGK4.5/ FGK45 anti-mouse CD40) and 10 ng/ml IL4. For rapamycin treatment, cells were activated as described above for 24 hours but in the presence of 20 nM rapamycin for the full duration of activation. For MYC inhibition, cells were activated as above in the presence of 5 μM MYCi361. Activated cells were FC blocked and stained with CD19 APC (for control and rapamycin treated cells) or CD19 APC-Cy7 (for control and MYCi361 treated cells) and DAPI, and live B cells were sorted and collected as described above. Gating strategy used for cell sorting is shown in Supplementary Figure 1. For iron chelation experiments lymphocytes were activated for 24 hours as described above but in the presence of deferiprone (3-Hydroxy-1,2-dimethyl-4(1H)-pyridone) at 10 μM, 50 μM, 100 μM and 300 μM. For flow cytometry analysis, samples were analysed on either a Novocyte or LSR Fortessa flow cytometer.

Flow cytometry assays for system-L amino acid uptake and protein synthesis

System-L amino acid uptake was measured using a single cell flow cytometry assay described previously [61]. In brief, after cell surface antibody staining non-stimulated and activated cells +/- rapamycin, were washed in pre-warmed HBSS and resuspended in 200μl HBSS. Cells were treated with either an inhibitor of system L transport 2-amino-2-norbornanecarboxylic (BCH) at a final concentration of 10mM or HBSS as a control. Kynurenine (KYN) was added to the cell suspension at a final concentration of 200μM. For live cell uptakes data was acquired on a flow cytometer immediately following KYN addition. KYN uptake was also assessed for a fixed time of 4 minutes after which time cells were fixed with paraformaldehyde at a final concentration of 1% and analysed by flow cytometry.

Rates of protein synthesis were measured using a click-chemistry reaction and flow cytometry. B cells were incubated for 20 minutes with O-propargyl-puromycin (OPP, Jena Bioscience), and the incorporation of the aminoacyl-tRNA mimetic into newly synthesized

polypeptides was measured by labelling the OPP was with Alexa 647-azide (Invitrogen) using a copper-catalysed click-chemistry reaction (Invitrogen). Cells were analysed using a LSR flow cytometer and analysed with FlowJo software (Treestar).

Proteomics sample preparation and peptide fractionation

Cell pellets were lysed in 400 µl of lysis buffer (5% sodium dodecyl sulfate, 50 mM triethylammonium bicarbonate (pH 8.5) and 10 mM tris(2-carboxyethyl)phosphine-hydrochloride). Lysates were shaken at room temperature at 1000 rpm for 5 minutes and then incubated at 95 °C at 500 rpm for 5 minutes. Samples were allowed to cool before being sonicated using a BioRuptor (15 cycles: 30 sec on and 30 sec off) and alkylated with 20 mM iodoacetamide for 1 h at 22 °C in the dark. Protein concentration was determined using the EZQ protein quantitation kit (Invitrogen) and protein cleanup and digestion was performed using S-TRAP mini columns (Protifi). Proteins were digested with trypsin trypsin at 1:20 ratio (enzyme:protein) for 2 hours at 47°C. Digested peptides were eluted from S-TRAP columns using 50mM ammonium bicarbonate, followed by 0.2% aqueous formic acid and 50% aqueous acetonitrile containing 0.2% formic acid. Peptides were dried by speedvac before resuspending in 1% formic acid for fractionation.

For naïve, activated and rapamycin B cell proteomes peptides were fractionated using high pH reverse-phase chromatography as described previously[62]. Samples were loaded onto a XbridgeTM BEH130 C18 column with 3.5 µm particles (Waters). Using a Dionex BioRS system, the samples were separated using a 25-min multistep gradient of solvents A (10 mM formate at pH 9 in 2% acetonitrile) and B (10 mM ammonium formate at pH 9 in 80% acetonitrile), at a flow rate of 0.3 ml/min. Peptides were separated into 16 fractions which were subsequently concatenated into 8. The fractions were dried and the peptides were dissolved in 1% formic acid and analyzed by liquid chromatography–mass spectrometry.

Liquid chromatography mass spectrometry analysis (LC- MS/MS)

For naïve, activated and rapamycin B cell proteomes samples were analysed by data dependent acquisition (DDA). 1.5 µg of peptide was injected onto a nanoscale C18 reverse-phase chromatography system (UltiMate 3000 RSLC nano, Thermo Scientific) and electrosprayed into an Q Exactive™ Plus mass spectrometer (Thermo Fisher) as described previously[63]. The following buffers were used for liquid chromatography: buffer A (0.1% formic acid in Milli-Q water (v/v)) and buffer B (80% acetonitrile and 0.1% formic acid in Milli-Q water (v/v). Samples were loaded at 10 µL/min onto a trap column (100 µm × 2 cm, PepMap nanoViper C18 column, 5 µm, 100 Å, Thermo Scientific) equilibrated in 0.1% trifluoroacetic acid (TFA). The trap column was washed for 3 min at the same flow rate with 0.1% TFA then switched in-line with a Thermo Scientific, resolving C18 column (75 µm × 50 cm, PepMap RSLC C18 column, 2 µm, 100 Å). Peptides were eluted from the column at a constant flow rate of 300 nl/min with a linear gradient from 3% buffer B to 6% buffer B in 5 min, then from 6% buffer B to 35% buffer B in 115 min, and finally to 80% buffer B within 7 min. The column was then washed with 80% buffer B for 4 min and re-equilibrated in 3% buffer B for 15 min. Two blanks were run between each sample to reduce carry-over. The column was kept at a constant temperature of 50°C.

The data was acquired using an easy spray source operated in positive mode with spray voltage at 2.445 kV, and the ion transfer tube temperature at 250°C. The MS was operated in DDA mode. A scan cycle comprised a full MS scan (m/z range from 350-1650), with RF lens at 40%, AGC target set to custom, normalised AGC target at 300, maximum injection time mode set to custom, maximum injection time at 20 ms and source fragmentation disabled. MS survey scan was followed by MS/MS DIA scan events using the following parameters: multiplex ions set to false, collision energy mode set to stepped, collision energy type set to normalized, HCD collision energies set to 25.5, 27 and 30, orbitrap resolution 30000, first mass 200, RF lens 40, AGC target set to custom, normalized AGC target 3000, maximum injection time 55 ms.

To generate proteomes examining the impact of MYC inhibition on B cells, peptides were analysed by data independent acquisition (DIA) as described previously [64–66]. 1.5 µg of peptides was injected onto a nanoscale C18 reverse-phase chromatography system (UltiMate 3000 RSLC nano, Thermo Scientific) and electrosprayed into an Orbitrap Exploris 480 Mass Spectrometer (Thermo Fisher). The following liquid chromatography buffers were used: buffer A (0.1% formic acid in Milli-Q water (v/v)) and buffer B (80% acetonitrile and 0.1% formic acid in Milli-Q water (v/v). Samples were loaded at 10 µl/min onto a trap column (100 µm × 2 cm, PepMap nanoViper C18 column, 5 µm, 100 Å, Thermo Scientific) equilibrated in 0.1% trifluoroacetic acid (TFA). The trap column was washed for 3 min at the same flow rate with 0.1% TFA then switched in-line with a Thermo Scientific, resolving C18 column (75 µm × 50 cm, PepMap RSLC C18 column, 2 µm, 100 Å). Peptides were eluted from the column at a constant flow rate of 300 nl/min with a linear gradient from 3% buffer B to 6% buffer B in 5 min, then from 6% buffer B to 35% buffer B in 115 min, and finally to 80% buffer B within 7 min. The column was then washed with 80% buffer B for 4 min and re-equilibrated in 3% buffer B for 15 min. Two blanks were run between each sample to reduce carry-over. The column was kept at a constant temperature of 50 °C.

The data was acquired using an easy spray source operated in positive mode with spray voltage at 2.445 kV, and the ion transfer tube temperature at 250 °C. The MS was operated in DIA mode. A scan cycle comprised a full MS scan (m/z range from 350 to 1650), with RF lens at 40%, AGC target set to custom, normalised AGC target at 300%, maximum injection time mode set to custom, maximum injection time at 20 ms, microscan set to 1 and source fragmentation disabled. MS survey scan was followed by MS/MS DIA scan events using the following parameters: multiplex ions set to false, collision energy mode set to stepped, collision energy type set to normalized, HCD collision energies set to 25.5, 27 and 30%, orbitrap resolution 30,000, first mass 200, RF lens 40%, AGC target set to custom,

normalized AGC target 3000%, microscan set to 1 and maximum injection time 55 ms. Data for both MS scan and MS/MS DIA scan events were acquired in profile mode.

Proteomics data processing and analysis

Data dependent mass spectrometry raw files were searched using MaxQuant[67] (version 1.6.10.43). Data was searched against a hybrid database from Uniprot release 06/2020. This hybrid database comprised of all manually annotated mouse SwissProt entries combined with mouse TrEMBL entries with protein level evidence available and a manually annotated homologue within the human SwissProt database. The false discovery rate was set to 1% for positive identification at the protein and peptide level. Protein N-terminal acetylation, methionine oxidation and deamidation (NQ) were set as variable modifications and carbamidomethylation of cysteine residues was selected as a fixed modification. Match between runs was disabled. Proteins categorized as ‘contaminants’, ‘reverse’ and ‘only identified by site’ were removed. Data independent mass spectrometry raw files were searched using Spectronaut (Biognosys) version 19. Raw mass spec files were searched against a mouse data base (Swissprot Trembl November 2023) with the following parameters: directDIA, false discovery rate set to 1%, protein N-terminal acetylation and methionine oxidation were set as variable modifications and carbamidomethylation of cysteine residues was selected as a fixed modification. Copy numbers were calculated using the proteomic ruler[12] using Perseus software[68]. GO term enrichment analysis was performed using the ORA algorithm from the R Bioconductor package clusterProfiler. The annotation database was set to GO biological process (GOBP) and the organism database used was org.Mm.eg.db (analysis run 8/12/2022). A secondary simplification step was performed to remove redundancies from GO enrichment results (default settings were used with a similarity cut-off of 0.6).

Statistics and calculations

For proteomics data, protein differential expression analysis was performed using R (v. 4.0.3) and p-values and fold changes were calculated using the Bioconductor package Limma (v 3.46.0)[69] . The q-value was calculated with the Bioconductor package qvalue (v 2.22.0).

Resource availability

All proteomics data is provided upon request. Raw mass spec data files and analysis files are available from the ProteomeXchange data repository upon publication.

Acknowledgments

The authors would like to thank the University of Dundee flow cytometry facility for cell sorting support and the University of Dundee Biological Resource Unit. We also thank Doreen Cantrell, Dana Cheung and Simon Arthur for helpful discussions. Animations were drawn using BioRender. This research was supported by Wellcome Trust grant 205023/Z/16/Z, and a Wellcome Trust Equipment Award, 202950/Z/16/Z.

Declaration of Interests

The authors declare no competing interests.

Author Contributions

AJMH, NL and LVS performed experiments. AJMH, LVS and FS designed experiments. OJ, LVS, NL, AB and AJMH analysed data. LVS, OJ and AJMH wrote the manuscript. All authors read and commented on the manuscript. AJMH conceived the project.

Figure legends

Figure 1 – Activation-induced proteome remodelling in B cells

(a) Flow cytometry forward scatter (FSC) profiles of naïve B cells (blue) and 24h anti-IGM, anti-CD40 and IL4-activated B cells (red, referred to as 'activated'). Data is representative of 3 biological replicates. **(b)** Total protein content (pg/cell) of naïve and 24h activated B cells. **(c)** Proteins ranked according to descending abundance and plotted against their cumulative abundance (shown as a percentage), for both naïve and 24h activated B cells. The number of proteins that make up each quartile of the proteome summed with the quartile below are shown on the designated section on each graph. Proteins making up the top-most 50% of activated B cells were annotated as either histones (orange), cytoskeletal (magenta), ribosomal (blue) or translational (pink) and were also mapped over the naïve B cell plot. **(d)** Top panel shows the total protein mass (pg/cell) of proteins belonging to cellular compartments including nuclear envelope (GOCC:0005635), plasma membrane (GOCC:0005886), mitochondria (GOCC:0005739) and ribosomes (KEGG 03010) as per Gene Ontology/KEGG Orthology terms. Lower panels show the % contribution to the total protein content for each term. **(e)** Differential expression analysis between naïve and activated B cells. Proteins were categorised as significantly changing between naïve and 24h activated B cells with a $P < 0.05$; fold change > 1.5 or found in one population but not detected in another population. Scatter plot shows the average protein copy number of each protein identified between naïve and 24h activated B cells. Proteins highlighted in red were significantly upregulated >1.5-fold between naïve and activated B cells, while proteins shown in blue were significantly downregulated. Proteins on the axes were found in one condition but not the other, numbers are provided on the plot for proteins found in 3/3 replicates of one condition. **(f)** Expression data for the cyclin dependent kinase inhibitor p27 (CDKN1B) and key regulators of the cell cycle. **(g)** Expression data for components of the eiF4F translational complex including the translational repressor PDCD4. **(h)** GO enrichment analysis of proteins significantly upregulated ($P < 0.05$ and fold change >5-fold) along with proteins only identified in activated B cells and absent in naïve B cells. The top 10 most enriched GOBP pathways are shown. **(i)** Schematic showing proteins enriched in the golgi vesicle transport pathway highlighted in the GO enrichment analysis shown in h. For e, f and

g statistical significance was derived from two-tailed empirical Bayes moderated t-statistics performed in limma on the total dataset where ** p<0.01, *** p<0.001. For b and d statistical significance was derived from an unpaired two-tailed t test where * p<0.05, ** p<0.01. All data are 3 biologically independent samples. All error bars are mean with s.d.

Figure 2 – The transcription factor profile of naïve and activated B cells

(a) Over 400 transcription factor and DNA-binding proteins were identified using the 'Human transcription factor' list (ref: https://doi.org/10.1016/j.cell.2018.01.029) as a reference database. Scatter plot compares copy number expression profiles of the transcription factors (blue) between naïve and 24h activated B cells against the total proteome (grey). Proteins were categorised as significantly changing between naïve and 24h activated B cells with a $P < 0.05$; fold change > 1.5 or found in one population but not detected in another population. Scatter plot shows the average protein copy number of each protein identified between naïve and 24h activated B cells. **(b)** Histograms showing protein copy numbers per cell for a selection of transcription factors such as those only expressed by activated B cells (newly synthesised), those with higher expression in activated as compared to naïve B cells (enhanced expression) and those only expressed by naïve B cells. Statistical significance was derived from two-tailed empirical Bayes moderated t-statistics performed in limma on the total dataset where *** p<0.001. All data are 3 biologically independent samples. All error bars are mean with s.d.

Figure 3 – B cell activation triggers metabolic and mitochondrial remodelling

(a) Boxplot showing the protein copy numbers per cell of a selection of amino acid transporters. **(b)** The impact of deleting the amino acid transporter SLC7A5 on B cell activation. Using flow cytometry, forward scatter and the expression of CD98 and CD71 was analysed in Vav cre^{+} Slc7a5$^{fl/fl}$ (SLC7A5 KO; red) and Vav cre^{-} Slc7a5$^{fl/fl}$ (SLC7A5 WT; blue) cells. B cells were activated with anti-IgM and anti-CD40 (activated) or maintained in IL-7 (no stim). **(c)** Schematic representation of the glycolytic pathway. Histograms show the protein

copy number per cell for the glucose transporter GLUT1 (SLC2A1) and the lactate transporter MCT1 (SLC16A1). Copy number expression of key enzymes involved in glycolysis and the pentose phosphate shuttle are represented as a heatmap (lower expression is represented by blue and higher expression is represented by red, proteins not detected are shown as grey). Also shown is the total protein content (pg/cell) of proteins involved in one carbon metabolism (GO:0006730). **(d)** >700 proteins were identified as belonging to the mitochondria as per the mouse MitoCarta 3.0 database [39]. Histogram shows the sum of all mitochondrial protein copy numbers per condition. A ratio for the contribution of each mitochondrial protein to the total was calculated by dividing the copy number of each protein by the total mitochondrial molecules. This ratio was used to the plot a heatmap showing relative expression from low (purple) to high (yellow). Heatmap was grouped based on the pathway annotations provided in MitoCarta 3.0. Histograms showing the protein copy numbers per cell, and associated ratio of the total, for proteins in particular pathways are shown. **(e)** Estimated copy numbers per cell for CD71(TFRC) in naïve and activated B cells. **(f)** The expression profile of proteins annotated as iron interacting (red circles) in naive versus activated B cells. **(g)** The estimated total iron atom requirement for those iron interacting proteins identified within naïve and activated B cells. For copy number comparisons of individual proteins statistical significance was derived from two-tailed empirical Bayes moderated t-statistics performed in limma on the total dataset where *** $p<0.001$. For all other comparisons statistical significance was derived from an unpaired two-tailed t test where * $p<0.05$, ** $p<0.01$, *** $p<0.001$. All data are 3 biologically independent samples except b which is representative of 2 biological repeats. All error bars are mean with s.d.

Figure 4 – The mTORC1 regulated proteome

(a) Phosphorylation of S6 in non-stimulated (grey), activated (black) and activated + rapamycin (red) cells, as determined by flow cytometry. **(b)** Flow cytometry forward scatter (FSC) profile of non-stimulated (grey), activated (black) and activated + rapamycin (red)

cells. **(c)** Total protein content (pg/cell) of naïve and 24h activated B cells +/- rapamycin. **(d)** Protein synthesis determined by O-propargyl-puromycin (OPP) incorporation into elongating protein chains and flow cytometry. **(e)** Volcano plot showing the differential expression profile of proteins as a consequence of rapamycin treatment. Data is presented as the log2 fold change of the copy number ratio (rapamycin treated vs untreated activated B cells) against the inverse significance value (-log10 P value). Proteins were considered significantly differentially expressed if the fold change value >1.5-fold in either an up- or down-regulated direction and if the P-value < 0.05 (significance cut off represented as a dashed line). **(f)** GO enrichment analysis of proteins significantly downregulated (P < 0.05 and-fold change >2-fold) plus proteins only identified in activated B cells and absent in rapamycin-treated B cells. Data shown are the top 10 most enriched GOBP pathways. **(g)** Total protein content (pg/cell) of proteins belonging to mitochondria (GOCC:0005739) and ribosomes (KEGG 03010). **(h)** Average copy number expression of a subset of transcription factors presented as a line plot between activated B cells +/- rapamycin. Key transcription factors controlling B cell identity and differentiation are shown. **(i)** Protein copy numbers for the Aryl Hydrocarbon receptor (AHR) and the Aryl hydrocarbon nuclear translocator (ARNT) in activated B cells +/- rapamycin. **(j)** Expression profile of solute carriers (SLC) proteins (orange) in response to rapamycin treatment. Log2 fold-change (rapamycin treated vs untreated activated B cells) is plotted against the inverse significance value (-log10 P value). P-value <0.05 represented as a dashed line. **(k)** Protein copy number per cell for a selection of key nutrient transporters for each condition: naïve, 24h activated and rapamycin-treated B cells. For e, i, j and k, differential expression analysis and statistical significance was derived from two-tailed empirical Bayes moderated t-statistics performed in limma on the total dataset where * p<0.05, ** p<0.01, *** p<0.001. For c and g, statistical significance was derived from an unpaired two-tailed t test where ** p<0.01. All data are 3 biologically independent samples. All error bars are mean with s.d. Data presented in d is representative of 3 biological replicates.

Figure 5 – mTORC1 activity regulates amino acid uptake, iron-interacting proteins and MYC expression

(a) Live flow cytometric monitoring of System L-dependent uptake in activated B cells +/- rapamycin. B cells were activated for 24 hours before the addition of the System L substrate kynurenine (KYN) and fluorescence emission (450 nm) monitored over time. Unstimulated cells were included as a control. **(b and c)** KYN uptake for 4 minutes and then fixed and analysed by flow cytometry. **(d and e)** The expression of CD98 in non-stimulated and activated B cells +/- rapamycin. **(f and g)** The expression of CD71 in non-stimulated and activated B cells +/- rapamycin. **(h)** The expression profile of iron-interacting proteins in naive, activated and activated + rapamycin B cells. A selection of iron-interacting protein categories are labelled on the heat map. **(i and j)** The impact of rapamycin treatment on MYC expression in activating B cells. B cells from GFP-tagged MYC mice were activated +/- rapamycin and MYC-GFP expression monitored at 4hrs and 24hrs by flow cytometry. Statistical significance was derived from an unpaired two-tailed t test where * $p<0.05$, *** $p<0.001$. For all experiments, 3 biologically independent samples were analysed.

Figure 6 – Blocking MYC activity impairs ribosomal protein mass and iron-interacting proteins

(a) Flow cytometry forward scatter (FSC) profile of non-stimulated (grey), activated (black) and activated + MYCi361 (green) cells. **(b)** Total protein molecules per cell for naïve and 24h activated B cells +/- MYCi361. **(c)** Volcano plot showing the differential expression profile of proteins as a consequence of MYCi361 treatment. Data is presented as the log2 fold change of the copy number ratio (MYCi361 treated vs untreated activated B cells) against the inverse significance value (-log10 P value). Proteins were considered significantly differentially expressed (highlighted in red) if the fold change value >1.5-fold in either up- or down-regulated direction and if the P-value < 0.05 (significance cut off represented as a dashed line). **(d)** Total ribosomal protein molecules per cell for naïve and 24h activated B cells +/- MYCi361. The impact of MYCi361 on CD62L (L-selectin), CD69 and CD71 (TFRC)

measured by mass spectrometry (**e**, **g** and **i**) and flow cytometry (**f**, **h** and **j**). **(k)** Volcano plot showing the expression profile of iron-interacting proteins in response to blocking MYC activity. For b, d, f, h and j statistical significance was derived from an unpaired two-tailed t test where * $p<0.05$, ** $p<0.01$. For all other experiments differential expression analysis and statistical significance was derived from two-tailed empirical Bayes moderated t-statistics performed in limma on the total dataset where * $p<0.05$, ** $p<0.01$. For all experiments, at least 3 biologically independent samples were analysed. All error bars are mean with s.d.

Figure 7 – Iron availability is critical for activation-induced B cell growth and protein synthesis

(a) Flow cytometry forward and side scatter profile of B cells after 24 hours either maintained in IL4 (1ng/ml) or activated with anti-IgM, anti CD40 and IL4 (10ng/ml) +/- the iron chelator deferiprone. **(b and c)** Forward scatter profile of B cells activated for 24 hours as described above. **(d and e)** CD69 expression in B cells after 24 hours either maintained in IL4 (1ng/ml) or activated with anti-IgM, anti CD40 and IL4 (10ng/ml) +/- deferiprone. **(f and g)** The impact of deferiprone on B cell protein synthesis. B cells were activated for 24 hours and protein synthesis measured by OPP incorporation and labelling with Alexa 647-azide using a copper-catalysed click-chemistry reaction. Cycloheximide was included as an inhibitor of cytosolic protein synthesis. For all experiments 3 biologically independent samples were analysed. All error bars are mean with s.d. Data in a, b, d and f are representative of 3 biological replicates. Statistical significance was derived from one way ANOVA where * $p<0.05$, ** $p<0.01$, *** $p<0.001$.

Supplementary Figures

Supplementary Figure 1 - Example gating strategy for cell sorting B cell populations

References

1. Liu, G.Y., and Sabatini, D.M. (2020). mTOR at the nexus of nutrition, growth, ageing and disease. Nat. Rev. Mol. Cell Biol. *21*, 183–203. https://doi.org/10.1038/s41580-019-0199-y.

2. Raybuck, A.L., Cho, S.H., Li, J., Rogers, M.C., Lee, K., Williams, C.L., Shlomchik, M., Thomas, J.W., Chen, J., Williams, J.V., et al. (2018). B Cell–Intrinsic mTORC1 Promotes Germinal Center–Defining Transcription Factor Gene Expression, Somatic Hypermutation, and Memory B Cell Generation in Humoral Immunity. J. Immunol. *200*, 2627–2639. https://doi.org/10.4049/jimmunol.1701321.

3. Iwata, T.N., Ramírez, J.A., Tsang, M., Park, H., Margineantu, D.H., Hockenbery, D.M., and Iritani, B.M. (2016). Conditional Disruption of Raptor Reveals an Essential Role for mTORC1 in B Cell Development, Survival, and Metabolism. J. Immunol. *197*, 2250–2260. https://doi.org/10.4049/jimmunol.1600492.

4. Zhang, S., Readinger, J.A., DuBois, W., Janka-Junttila, M., Robinson, R., Pruitt, M., Bliskovsky, V., Wu, J.Z., Sakakibara, K., Patel, J., et al. (2011). Constitutive reductions in mTOR alter cell size, immune cell development, and antibody production. Blood *117*, 1228–1238. https://doi.org/10.1182/blood-2010-05-287821.

5. Iwata, T.N., Ramírez-Komo, J.A., Park, H., and Iritani, B.M. (2017). Control of B lymphocyte development and functions by the mTOR signaling pathways. Cytokine Growth Factor Rev. *35*, 47–62. https://doi.org/10.1016/j.cytogfr.2017.04.005.

6. Gaudette, B.T., Jones, D.D., Bortnick, A., Argon, Y., and Allman, D. (2020). mTORC1 coordinates an immediate unfolded protein response-related transcriptome in activated B cells preceding antibody secretion. Nat. Commun. *11*, 723. https://doi.org/10.1038/s41467-019-14032-1.

7. Tan, H., Yang, K., Li, Y., Shaw, T.I., Wang, Y., Blanco, D.B., Wang, X., Cho, J.-H., Wang, H., Rankin, S., et al. (2017). Integrative Proteomics and Phosphoproteomics Profiling Reveals Dynamic Signaling Networks and Bioenergetics Pathways Underlying T Cell Activation. Immunity *46*, 488–503. https://doi.org/10.1016/j.immuni.2017.02.010.

8. Rieckmann, J.C., Geiger, R., Hornburg, D., Wolf, T., Kveler, K., Jarrossay, D., Sallusto, F., Shen-Orr, S.S., Lanzavecchia, A., Mann, M., et al. (2017). Social network architecture of human immune cells unveiled by quantitative proteomics. Nat. Immunol. *18*, 583–593. https://doi.org/10.1038/ni.3693.

9. Salerno, F., Howden, A.J.M., Matheson, L.S., Gizlenci, Ö., Screen, M., Lingel, H., Brunner-Weinzierl, M.C., and Turner, M. (2023). An integrated proteome and transcriptome of B cell maturation defines poised activation states of transitional and mature B cells. Nat. Commun. *14*, 5116. https://doi.org/10.1038/s41467-023-40621-2.

10. Hukelmann, J.L., Anderson, K.E., Sinclair, L.V., Grzes, K.M., Murillo, A.B., Hawkins, P.T., Stephens, L.R., Lamond, A.I., and Cantrell, D.A. (2016). The cytotoxic T cell proteome and its shaping by the kinase mTOR. Nat. Immunol. *17*, 104–112. https://doi.org/10.1038/ni.3314.

11. Brenes, A.J., Lamond, A.I., and Cantrell, D.A. (2023). The Immunological Proteome Resource. Nat. Immunol. *24*, 731–731. https://doi.org/10.1038/s41590-023-01483-4.

12. Wiśniewski, J.R., Hein, M.Y., Cox, J., and Mann, M. (2014). A “Proteomic Ruler” for Protein Copy Number and Concentration Estimation without Spike-in Standards*. Mol. Cell. Proteom.□: MCP *13*, 3497–3506. https://doi.org/10.1074/mcp.m113.037309.

13. Winkelmann, R., Sandrock, L., Kirberg, J., Jäck, H.-M., and Schuh, W. (2014). KLF2– A Negative Regulator of Pre-B Cell Clonal Expansion and B Cell Activation. PLoS ONE *9*, e97953. https://doi.org/10.1371/journal.pone.0097953.

14. Hart, G.T., Wang, X., Hogquist, K.A., and Jameson, S.C. (2011). Krüppel-like factor 2 (KLF2) regulates B-cell reactivity, subset differentiation, and trafficking molecule expression. Proc. Natl. Acad. Sci. *108*, 716–721. https://doi.org/10.1073/pnas.1013168108.

15. Wittner, J., and Schuh, W. (2023). Krüppel-like factor 2: a central regulator of B cell differentiation and plasma cell homing. Front. Immunol. *14*, 1172641. https://doi.org/10.3389/fimmu.2023.1172641.

16. Suzuki, C., Garces, R.G., Edmonds, K.A., Hiller, S., Hyberts, S.G., Marintchev, A., and Wagner, G. (2008). PDCD4 inhibits translation initiation by binding to eIF4A using both its MA3 domains. Proc. Natl. Acad. Sci. *105*, 3274–3279. https://doi.org/10.1073/pnas.0712235105.

17. Loh, P.G., Yang, H., Walsh, M.A., Wang, Q., Wang, X., Cheng, Z., Liu, D., and Song, H. (2009). Structural basis for translational inhibition by the tumour suppressor Pdcd4. EMBO J. *28*, 274–285. https://doi.org/10.1038/emboj.2008.278.

18. Barlowe, C., Orci, L., Yeung, T., Hosobuchi, M., Hamamoto, S., Salama, N., Rexach, M.F., Ravazzola, M., Amherdt, M., and Schekman, R. (1994). COPII: A membrane coat formed by Sec proteins that drive vesicle budding from the endoplasmic reticulum. Cell *77*, 895–907. https://doi.org/10.1016/0092-8674(94)90138-4.

19. Miller, E., Antonny, B., Hamamoto, S., and Schekman, R. (2002). Cargo selection into COPII vesicles is driven by the Sec24p subunit. EMBO J. *21*, 6105–6113. https://doi.org/10.1093/emboj/cdf605.

20. Bi, X., Mancias, J.D., and Goldberg, J. (2007). Insights into COPII Coat Nucleation from the Structure of Sec23•Sar1 Complexed with the Active Fragment of Sec31. Dev. Cell *13*, 635–645. https://doi.org/10.1016/j.devcel.2007.10.006.

21. Fath, S., Mancias, J.D., Bi, X., and Goldberg, J. (2007). Structure and Organization of Coat Proteins in the COPII Cage. Cell *129*, 1325–1336. https://doi.org/10.1016/j.cell.2007.05.036.

22. Kashiwada, M., Levy, D.M., McKeag, L., Murray, K., Schröder, A.J., Canfield, S.M., Traver, G., and Rothman, P.B. (2010). IL-4-induced transcription factor NFIL3/E4BP4 controls IgE class switching. Proc. Natl. Acad. Sci. *107*, 821–826. https://doi.org/10.1073/pnas.0909235107.

23. Li, S., Miao, T., Sebastian, M., Bhullar, P., Ghaffari, E., Liu, M., Symonds, A.L.J., and Wang, P. (2012). The Transcription Factors Egr2 and Egr3 Are Essential for the Control of Inflammation and Antigen-Induced Proliferation of B and T Cells. Immunity *37*, 685–696. https://doi.org/10.1016/j.immuni.2012.08.001.

24. Cobaleda, C., Schebesta, A., Delogu, A., and Busslinger, M. (2007). Pax5: the guardian of B cell identity and function. Nat. Immunol. *8*, 463–470. https://doi.org/10.1038/ni1454.

25. Fedl, A.S., Tagoh, H., Gruenbacher, S., Sun, Q., Schenk, R.L., Froussios, K., Jaritz, M., Busslinger, M., and Schwickert, T.A. (2024). Transcriptional function of E2A, Ebf1, Pax5, Ikaros and Aiolos analyzed by in vivo acute protein degradation in early B cell development. Nat. Immunol. *25*, 1663–1677. https://doi.org/10.1038/s41590-024-01933-7.

26. Scalise, M., Pochini, L., Console, L., Losso, M.A., and Indiveri, C. (2018). The Human SLC1A5 (ASCT2) Amino Acid Transporter: From Function to Structure and Role in Cell Biology. Frontiers Cell Dev Biology *6*, 96. https://doi.org/10.3389/fcell.2018.00096.

27. Kanai, Y., Segawa, H., Miyamoto, K., Uchino, H., Takeda, E., and Endou, H. (1998). Expression Cloning and Characterization of a Transporter for Large Neutral Amino Acids Activated by the Heavy Chain of 4F2 Antigen (CD98)*. J Biol Chem *273*, 23629–23632. https://doi.org/10.1074/jbc.273.37.23629.

28. Sinclair, L.V., Rolf, J., Emslie, E., Shi, Y.-B., Taylor, P.M., and Cantrell, D.A. (2013). Control of amino-acid transport by antigen receptors coordinates the metabolic reprogramming essential for T cell differentiation. Nat. Immunol. *14*, 500–508. https://doi.org/10.1038/ni.2556.

29. Sinclair, L.V., Howden, A.J., Brenes, A., Spinelli, L., Hukelmann, J.L., Macintyre, A.N., Liu, X., Thomson, S., Taylor, P.M., Rathmell, J.C., et al. (2019). Antigen receptor control of methionine metabolism in T cells. eLife *8*, 1132. https://doi.org/10.7554/elife.44210.

30. Palacín, M., and Kanai, Y. (2004). The ancillary proteins of HATs: SLC3 family of amino acid transporters. Pflügers Arch. *447*, 490–494. https://doi.org/10.1007/s00424-003-1062-7.

31. Jabara, H.H., Boyden, S.E., Chou, J., Ramesh, N., Massaad, M.J., Benson, H., Bainter, W., Fraulino, D., Rahimov, F., Sieff, C., et al. (2016). A missense mutation in TFRC, encoding transferrin receptor 1, causes combined immunodeficiency. Nat Genet *48*, 74–78. https://doi.org/10.1038/ng.3465.

32. Neckers, L.M., Yenokida, G., and James, S.P. (1984). The role of the transferrin receptor in human B lymphocyte activation. J. Immunol. (Baltim., Md□: 1950) *133*, 2437–2441.

33. Frost, J.N., Tan, T.K., Abbas, M., Wideman, S.K., Bonadonna, M., Stoffel, N.U., Wray, K., Kronsteiner, B., Smits, G., Campagna, D.R., et al. (2020). Hepcidin-Mediated Hypoferremia Disrupts Immune Responses to Vaccination and Infection. Med, 1–29. https://doi.org/10.1016/j.medj.2020.10.004.

34. Boothby, M., and Rickert, R.C. (2017). Metabolic Regulation of the Immune Humoral Response. Immunity *46*, 743–755. https://doi.org/10.1016/j.immuni.2017.04.009.

35. Waters, L.R., Ahsan, F.M., Wolf, D.M., Shirihai, O., and Teitell, M.A. (2018). Initial B Cell Activation Induces Metabolic Reprogramming and Mitochondrial Remodeling. iScience *5*, 99–109. https://doi.org/10.1016/j.isci.2018.07.005.

36. Tanner, L.B., Goglia, A.G., Wei, M.H., Sehgal, T., Parsons, L.R., Park, J.O., White, E., Toettcher, J.E., and Rabinowitz, J.D. (2018). Four Key Steps Control Glycolytic Flux in Mammalian Cells. Cell Syst. *7*, 49-62.e8. https://doi.org/10.1016/j.cels.2018.06.003.

37. Yazicioglu, Y.F., Marin, E., Sandhu, C., Galiani, S., Raza, I.G.A., Ali, M., Kronsteiner, B., Compeer, E.B., Attar, M., Dunachie, S.J., et al. (2023). Dynamic mitochondrial transcription and translation in B cells control germinal center entry and lymphomagenesis. Nat. Immunol. *24*, 991–1006. https://doi.org/10.1038/s41590-023-01484-3.

38. Iborra-Pernichi, M., García, J.R., Esperanza, M.V. de la, Estrada, B.S., Bovolenta, E.R., Cifuentes, C., Carro, C.P., Martínez, T.G., García-Consuegra, J., Rey-Stolle, M.F., et al. (2024). Defective mitochondria remodelling in B cells leads to an aged immune response. Nat. Commun. *15*, 2569. https://doi.org/10.1038/s41467-024-46763-1.

39. Rath, S., Sharma, R., Gupta, R., Ast, T., Chan, C., Durham, T.J., Goodman, R.P., Grabarek, Z., Haas, M.E., Hung, W.H.W., et al. (2020). MitoCarta3.0: an updated mitochondrial proteome now with sub-organelle localization and pathway annotations. Nucleic Acids Res. *49*, D1541–D1547. https://doi.org/10.1093/nar/gkaa1011.

40. Teh, M.R., Frost, J.N., Armitage, A.E., and Drakesmith, H. (2021). Analysis of Iron and Iron-Interacting Protein Dynamics During T-Cell Activation. Front. Immunol. *12*, 714613. https://doi.org/10.3389/fimmu.2021.714613.

41. Howden, A.J., Hukelmann, J.L., Brenes, A., Spinelli, L., Sinclair, L.V., Lamond, A.I., and Cantrell, D.A. (2019). Quantitative analysis of T cell proteomes and environmental sensors during T cell differentiation. Nat. Immunol. *20*, 1542–1554. https://doi.org/10.1038/s41590-019-0495-x.

42. Chi, H. (2012). Regulation and function of mTOR signalling in T cell fate decisions. Nat. Rev. Immunol. *12*, 325–338. https://doi.org/10.1038/nri3198.

43. Pollizzi, K.N., and Powell, J.D. (2015). Regulation of T cells by mTOR: the known knowns and the known unknowns. Trends Immunol. *36*, 13–20. https://doi.org/10.1016/j.it.2014.11.005.

44. Goul, C., Peruzzo, R., and Zoncu, R. (2023). The molecular basis of nutrient sensing and signalling by mTORC1 in metabolism regulation and disease. Nat. Rev. Mol. Cell Biol. *24*, 857–875. https://doi.org/10.1038/s41580-023-00641-8.

45. Patterson, D.G., Kania, A.K., Price, M.J., Rose, J.R., Scharer, C.D., and Boss, J.M. (2021). An IRF4–MYC–mTORC1 Integrated Pathway Controls Cell Growth and the Proliferative Capacity of Activated B Cells during B Cell Differentiation In Vivo. J. Immunol. *207*, 1798–1811. https://doi.org/10.4049/jimmunol.2100440.

46. Wang, H., Lee, C.H., Qi, C., Tailor, P., Feng, J., Abbasi, S., Atsumi, T., and Morse, H.C. (2008). IRF8 regulates B-cell lineage specification, commitment, and differentiation. Blood *112*, 4028–4038. https://doi.org/10.1182/blood-2008-01-129049.

47. Lee, C.H., Melchers, M., Wang, H., Torrey, T.A., Slota, R., Qi, C.-F., Kim, J.Y., Lugar, P., Kong, H.J., Farrington, L., et al. (2006). Regulation of the germinal center gene program by interferon (IFN) regulatory factor 8/IFN consensus sequence-binding protein. J. Exp. Med. *203*, 63–72. https://doi.org/10.1084/jem.20051450.

48. Wang, H., Jain, S., Li, P., Lin, J.-X., Oh, J., Qi, C., Gao, Y., Sun, J., Sakai, T., Naghashfar, Z., et al. (2019). Transcription factors IRF8 and PU.1 are required for follicular B cell development and BCL6-driven germinal center responses. Proc. Natl. Acad. Sci. *116*, 9511–9520. https://doi.org/10.1073/pnas.1901258116.

49. Villa, M., Gialitakis, M., Tolaini, M., Ahlfors, H., Henderson, C.J., Wolf, C.R., Brink, R., and Stockinger, B. (2017). Aryl hydrocarbon receptor is required for optimal B-cell proliferation. EMBO J. *36*, 116–128. https://doi.org/10.15252/embj.201695027.

50. Sinclair, L.V., Neyens, D., Ramsay, G., Taylor, P.M., and Cantrell, D.A. (2018). Single cell analysis of kynurenine and System L amino acid transport in T cells. Nature Communications, 1–11. https://doi.org/10.1038/s41467-018-04366-7.

51. Marchingo, J.M., Sinclair, L.V., Howden, A.J., and Cantrell, D.A. (2020). Quantitative analysis of how Myc controls T cell proteomes and metabolic pathways during T cell activation. eLife *9*, e53725. https://doi.org/10.7554/elife.53725.

52. Nie, Z., Hu, G., Wei, G., Cui, K., Yamane, A., Resch, W., Wang, R., Green, D.R., Tessarollo, L., Casellas, R., et al. (2012). c-Myc Is a Universal Amplifier of Expressed Genes in Lymphocytes and Embryonic Stem Cells. Cell *151*, 68–79. https://doi.org/10.1016/j.cell.2012.08.033.

53. Han, H., Jain, A.D., Truica, M.I., Izquierdo-Ferrer, J., Anker, J.F., Lysy, B., Sagar, V., Luan, Y., Chalmers, Z.R., Unno, K., et al. (2019). Small-Molecule MYC Inhibitors Suppress Tumor Growth and Enhance Immunotherapy. Cancer Cell *36*, 483-497.e15. https://doi.org/10.1016/j.ccell.2019.10.001.

54. Preston, G.C., Sinclair, L.V., Kaskar, A., Hukelmann, J.L., Navarro, M.N., Ferrero, I., MacDonald, H.R., Cowling, V.H., and Cantrell, D.A. (2015). Single cell tuning of Myc expression by antigen receptor signal strength and interleukin-2 in T lymphocytes. EMBO J. *34*, 2008–2024. https://doi.org/10.15252/embj.201490252.

55. O'Donnell, K.A., Yu, D., Zeller, K.I., Kim, J., Racke, F., Thomas-Tikhonenko, A., and Dang, C.V. (2006). Activation of Transferrin Receptor 1 by c-Myc Enhances Cellular Proliferation and Tumorigenesis. Mol. Cell. Biol. *26*, 2373–2386. https://doi.org/10.1128/mcb.26.6.2373-2386.2006.

56. Sun, Y., Wen, J., Xu, T., and Meng, L. (2023). Reduction of peritoneal cavity B1a cells in adult Slc7a5 knockdown mice via dysregulating the mTOR pathway. Int. Immunopharmacol. *117*, 109939. https://doi.org/10.1016/j.intimp.2023.109939.

57. Ben-Sahra, I., and Manning, B.D. (2017). mTORC1 signaling and the metabolic control of cell growth. Curr. Opin. Cell Biol. *45*, 72–82. https://doi.org/10.1016/j.ceb.2017.02.012.

58. Valvezan, A.J., and Manning, B.D. (2019). Molecular logic of mTORC1 signalling as a metabolic rheostat. Nat. Metab. *1*, 321–333. https://doi.org/10.1038/s42255-019-0038-7.

59. Ned, R.M., Swat, W., and Andrews, N.C. (2003). Transferrin receptor 1 is differentially required in lymphocyte development. Blood *102*, 3711–3718. https://doi.org/10.1182/blood-2003-04-1086.

60. Stoffel, N.U., and Drakesmith, H. (2024). Effects of Iron Status on Adaptive Immunity and Vaccine Efficacy: A Review. Adv. Nutr. *15*, 100238. https://doi.org/10.1016/j.advnut.2024.100238.

61. Sinclair, L.V., Neyens, D., Ramsay, G., Taylor, P.M., and Cantrell, D.A. (2018). Single cell analysis of kynurenine and System L amino acid transport in T cells. Nature Communications, 1–11. https://doi.org/10.1038/s41467-018-04366-7.

62. Damasio, M.P., Marchingo, J.M., Spinelli, L., Hukelmann, J.L., Cantrell, D.A., and Howden, A.J.M. (2021). Extracellular signal-regulated kinase (ERK) pathway control of CD8+ T cell differentiation. Biochem. J. *478*, 79–98. https://doi.org/10.1042/bcj20200661.

63. Lloyd, A.F., Martinez-Muriana, A., Davis, E., Daniels, M.J.D., Hou, P., Mancuso, R., Brenes, A.J., Sinclair, L.V., Geric, I., Snellinx, A., et al. (2024). Deep proteomic analysis of microglia reveals fundamental biological differences between model systems. Cell Rep. *43*, 114908. https://doi.org/10.1016/j.celrep.2024.114908.

64. Molina-Gonzalez, I., Holloway, R.K., Jiwaji, Z., Dando, O., Kent, S.A., Emelianova, K., Lloyd, A.F., Forbes, L.H., Mahmood, A., Skripuletz, T., et al. (2023). Astrocyte-oligodendrocyte interaction regulates central nervous system regeneration. Nat. Commun. *14*, 3372. https://doi.org/10.1038/s41467-023-39046-8.

65. Walgrave, H., Penning, A., Tosoni, G., Snoeck, S., Davie, K., Davis, E., Wolfs, L., Sierksma, A., Mars, M., Bu, T., et al. (2023). microRNA-132 regulates gene expression programs involved in microglial homeostasis. iScience *26*, 106829. https://doi.org/10.1016/j.isci.2023.106829.

66. Sollberger, G., Brenes, A.J., Warner, J., Arthur, J.S.C., and Howden, A.J.M. (2024). Quantitative proteomics reveals tissue-specific, infection-induced and species-specific neutrophil protein signatures. Sci. Rep. *14*, 5966. https://doi.org/10.1038/s41598-024-56163-6.

67. Cox, J., and Mann, M. (2008). MaxQuant enables high peptide identification rates, individualized p.p.b.-range mass accuracies and proteome-wide protein quantification. Nat. Biotechnol. *26*, 1367–1372. https://doi.org/10.1038/nbt.1511.

68. Tyanova, S., Temu, T., Sinitcyn, P., Carlson, A., Hein, M.Y., Geiger, T., Mann, M., and Cox, J. (2016). The Perseus computational platform for comprehensive analysis of (prote)omics data. Nat. Methods *13*, 731–740. https://doi.org/10.1038/nmeth.3901.

69. Ritchie, M.E., Phipson, B., Wu, D., Hu, Y., Law, C.W., Shi, W., and Smyth, G.K. (2015). limma powers differential expression analyses for RNA-sequencing and microarray studies. Nucleic Acids Res. *43*, e47–e47. https://doi.org/10.1093/nar/gkv007.

Figure 1

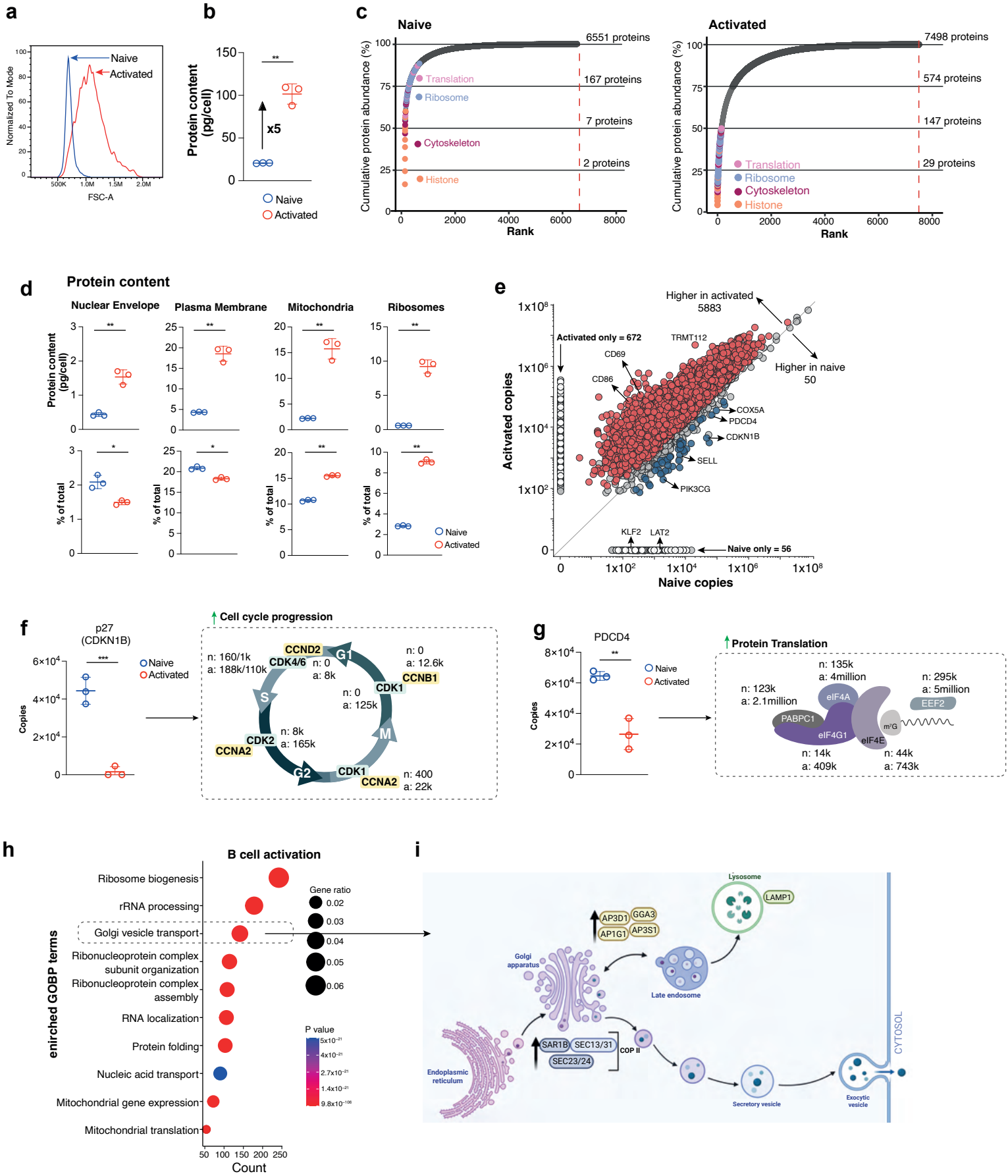
a
Naive
Activated
Normalized To Mode
FSC-A
b
Protein content (pg/cell)
x5
Naive
Activated
c
Naive
Activated
Cumulative protein abundance (%)
Rank
6551 proteins
167 proteins
7 proteins
2 proteins
7498 proteins
574 proteins
147 proteins
29 proteins
Translation
Ribosome
Cytoskeleton
Histone
d
Protein content
Nuclear Envelope
Plasma Membrane
Mitochondria
Ribosomes
Protein content (pg/cell)
% of total
Naive
Activated
e
Higher in activated 5883
Higher in naive 50
Activated only = 672
Naive only = 56
Acitvated copies
Naive copies
TRMT112
CD69
CD86
COX5A
PDCD4
CDKN1B
SELL
PIK3CG
KLF2
LAT2
f
p27 (CDKN1B)
Naive
Activated
Copies
Cell cycle progression
CCND2
CDK4/6
CCNB1
CDK1
CDK2
CCNA2
G1
S
G2
M
n: 160/1k
a: 188k/110k
n: 0
a: 8k
n: 0
a: 12.6k
n: 0
a: 125k
n: 8k
a: 165k
n: 400
a: 22k
g
PDCD4
Naive
Activated
Copies
Protein Translation
n: 123k
a: 2.1million
n: 135k
a: 4million
n: 295k
a: 5million
n: 14k
a: 409k
n: 44k
a: 743k
PABPC1
eIF4A
eIF4G1
eIF4E
EEF2
m7G
h
B cell activation
enirched GOBP terms
Ribosome biogenesis
rRNA processing
Golgi vesicle transport
Ribonucleoprotein complex subunit organization
Ribonucleoprotein complex assembly
RNA localization
Protein folding
Nucleic acid transport
Mitochondrial gene expression
Mitochondrial translation
Gene ratio
0.02
0.03
0.04
0.05
0.06
P value
Count
i
Lysosome
LAMP1
AP3D1
GGA3
AP1G1
AP3S1
Golgi apparatus
Late endosome
SAR1B
SEC13/31
SEC23/24
COP II
Endoplasmic reticulum
Secretory vesicle
Exocytic vesicle
CYTOSOL

Figure 2

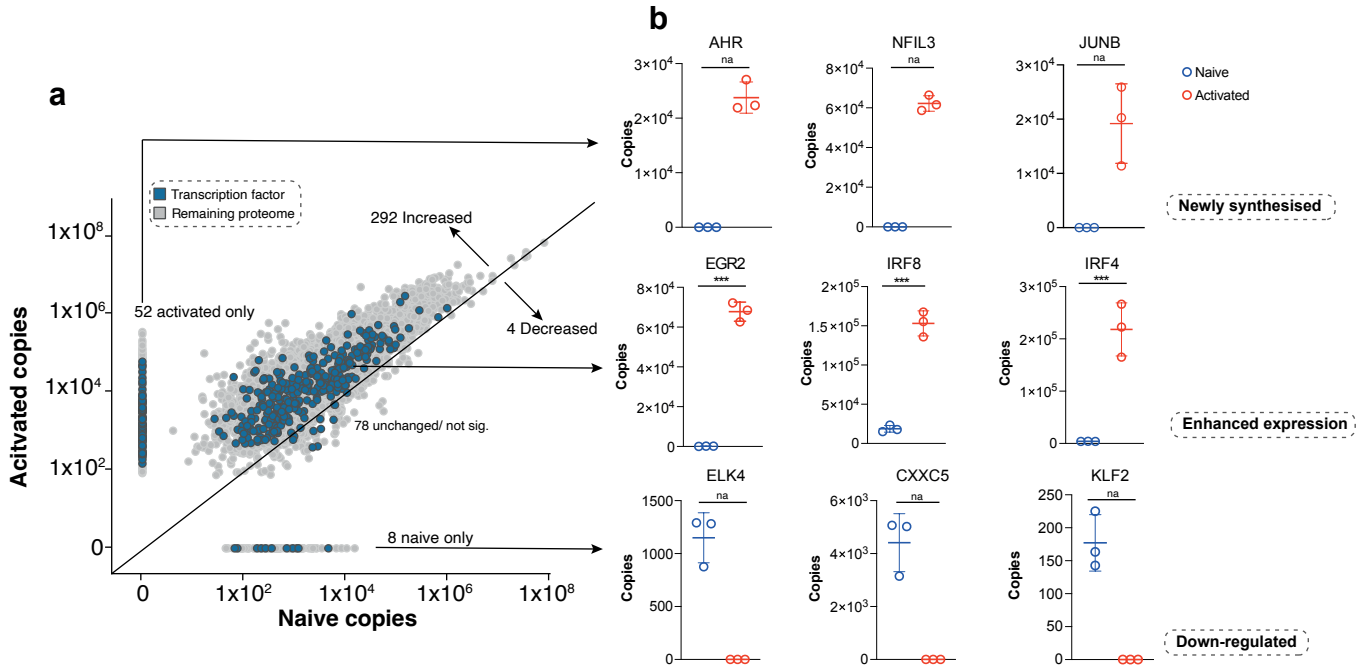
a
b
Transcription factor
Remaining proteome
292 Increased
4 Decreased
52 activated only
78 unchanged/ not sig.
8 naive only
Acitvated copies
Naive copies
AHR
NFIL3
JUNB
EGR2
IRF8
IRF4
ELK4
CXXC5
KLF2
Copies
Naive
Activated
Newly synthesised
Enhanced expression
Down-regulated

Figure 3

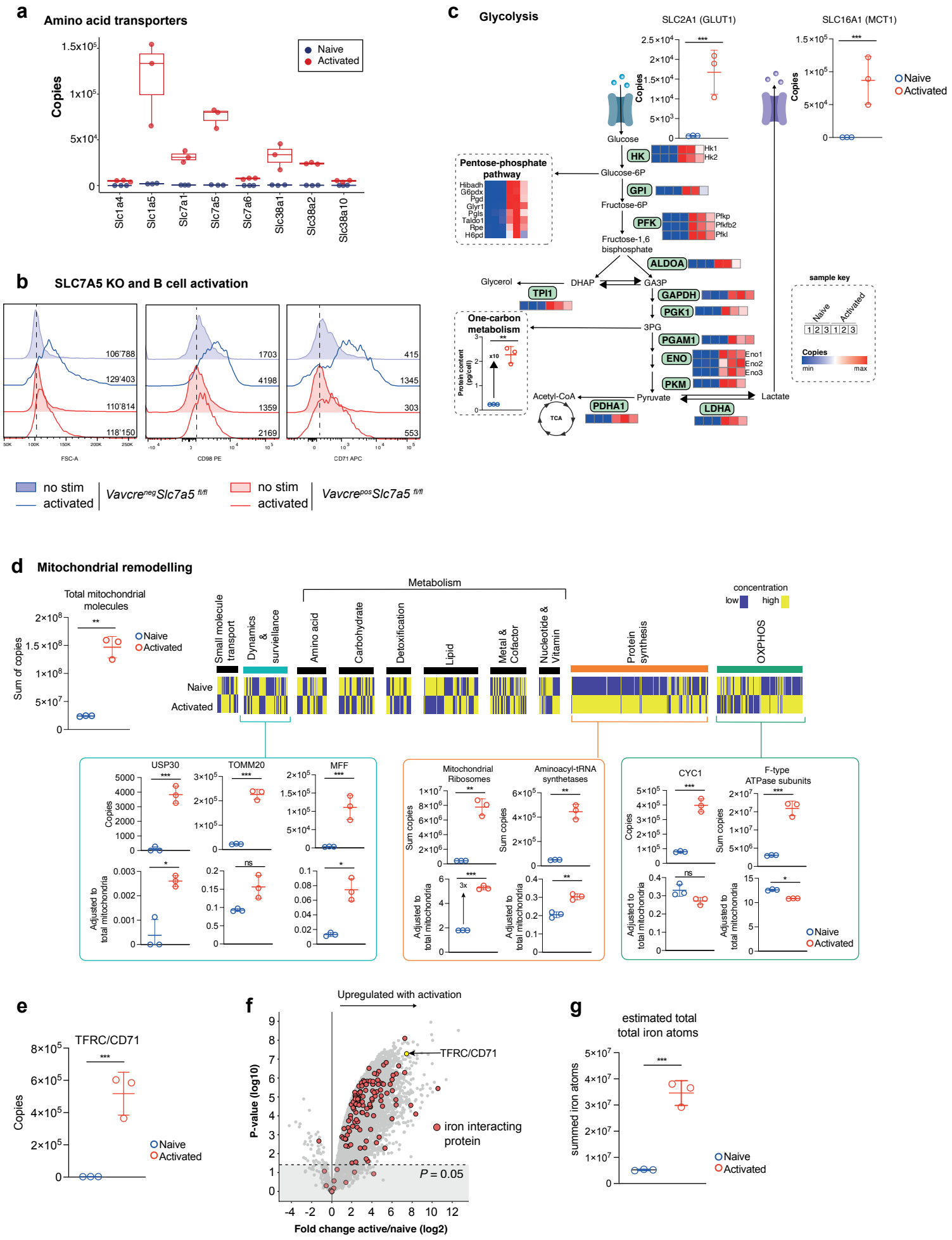
a
Amino acid transporters
Copies
Naive
Activated
Slc1a4
Slc1a5
Slc7a1
Slc7a5
Slc7a6
Slc38a1
Slc38a2
Slc38a10
b
SLC7A5 KO and B cell activation
106'788
129'403
110'814
118'150
1703
4198
1359
2169
415
1345
303
553
FSC-A
CD98 PE
CD71 APC
no stim
activated
Vavcre^neg Slc7a5 fl/fl
no stim
activated
Vavcre^pos Slc7a5 fl/fl
c
Glycolysis
SLC2A1 (GLUT1)
SLC16A1 (MCT1)
Glucose
HK
Hk1
Hk2
Glucose-6P
GPI
Fructose-6P
PFK
Pfkp
Pfkfb2
Pfkl
Fructose-1,6 bisphosphate
ALDOA
DHAP
GA3P
Glycerol
TPI1
GAPDH
PGK1
3PG
PGAM1
ENO
Eno1
Eno2
Eno3
PKM
Pyruvate
Lactate
LDHA
Acetyl-CoA
PDHA1
TCA
Pentose-phosphate pathway
Hibadh
G6pdx
Pgd
Glyr1
Pgls
Taldo1
Rpe
H6pd
One-carbon metabolism
Protein content (pg/cell)
x10
sample key
Naive
Activated
Copies
min
max
d
Mitochondrial remodelling
Total mitochondrial molecules
Sum of copies
Naive
Activated
Metabolism
Small molecule transport
Dynamics & surveillance
Amino acid
Carbohydrate
Detoxification
Lipid
Metal & Cofactor
Nucleotide & Vitamin
Protein synthesis
OXPHOS
concentration
low
high
USP30
TOMM20
MFF
Copies
Adjusted to total mitochondria
Mitochondrial Ribosomes
Aminoacyl-tRNA synthetases
Sum copies
CYC1
F-type ATPase subunits
e
TFRC/CD71
Copies
Naive
Activated
f
Upregulated with activation
TFRC/CD71
iron interacting protein
P = 0.05
P-value (log10)
Fold change active/naive (log2)
g
estimated total total iron atoms
summed iron atoms
Naive
Activated

Figure 4

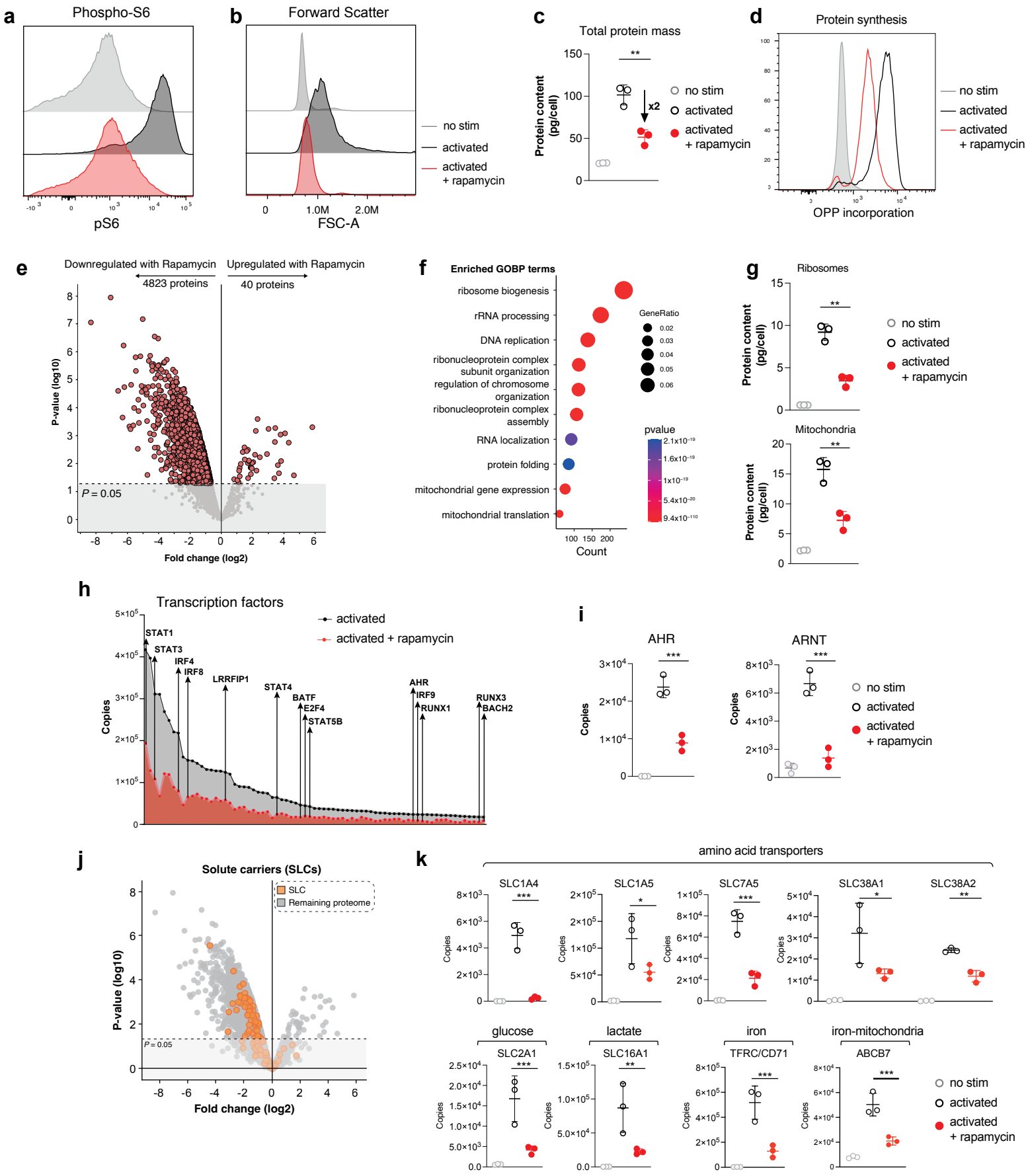
a
Phospho-S6
pS6
b
Forward Scatter
FSC-A
no stim
activated
activated + rapamycin
c
Total protein mass
Protein content (pg/cell)
x2
no stim
activated
activated + rapamycin
d
Protein synthesis
OPP incorporation
e
Downregulated with Rapamycin
4823 proteins
Upregulated with Rapamycin
40 proteins
P-value (log10)
P = 0.05
Fold change (log2)
f
Enriched GOBP terms
ribosome biogenesis
rRNA processing
DNA replication
ribonucleoprotein complex subunit organization
regulation of chromosome organization
ribonucleoprotein complex assembly
RNA localization
protein folding
mitochondrial gene expression
mitochondrial translation
GeneRatio
pvalue
Count
g
Ribosomes
Mitochondria
Protein content (pg/cell)
no stim
activated
activated + rapamycin
h
Transcription factors
activated
activated + rapamycin
Copies
STAT1
STAT3
IRF4
IRF8
LRRFIP1
STAT4
BATF
E2F4
STAT5B
AHR
IRF9
RUNX1
RUNX3
BACH2
i
AHR
ARNT
Copies
no stim
activated
activated + rapamycin
j
Solute carriers (SLCs)
SLC
Remaining proteome
P-value (log10)
P = 0.05
Fold change (log2)
k
amino acid transporters
SLC1A4
SLC1A5
SLC7A5
SLC38A1
SLC38A2
glucose
SLC2A1
lactate
SLC16A1
iron
TFRC/CD71
iron-mitochondria
ABCB7
Copies
no stim
activated
activated + rapamycin

Figure 5

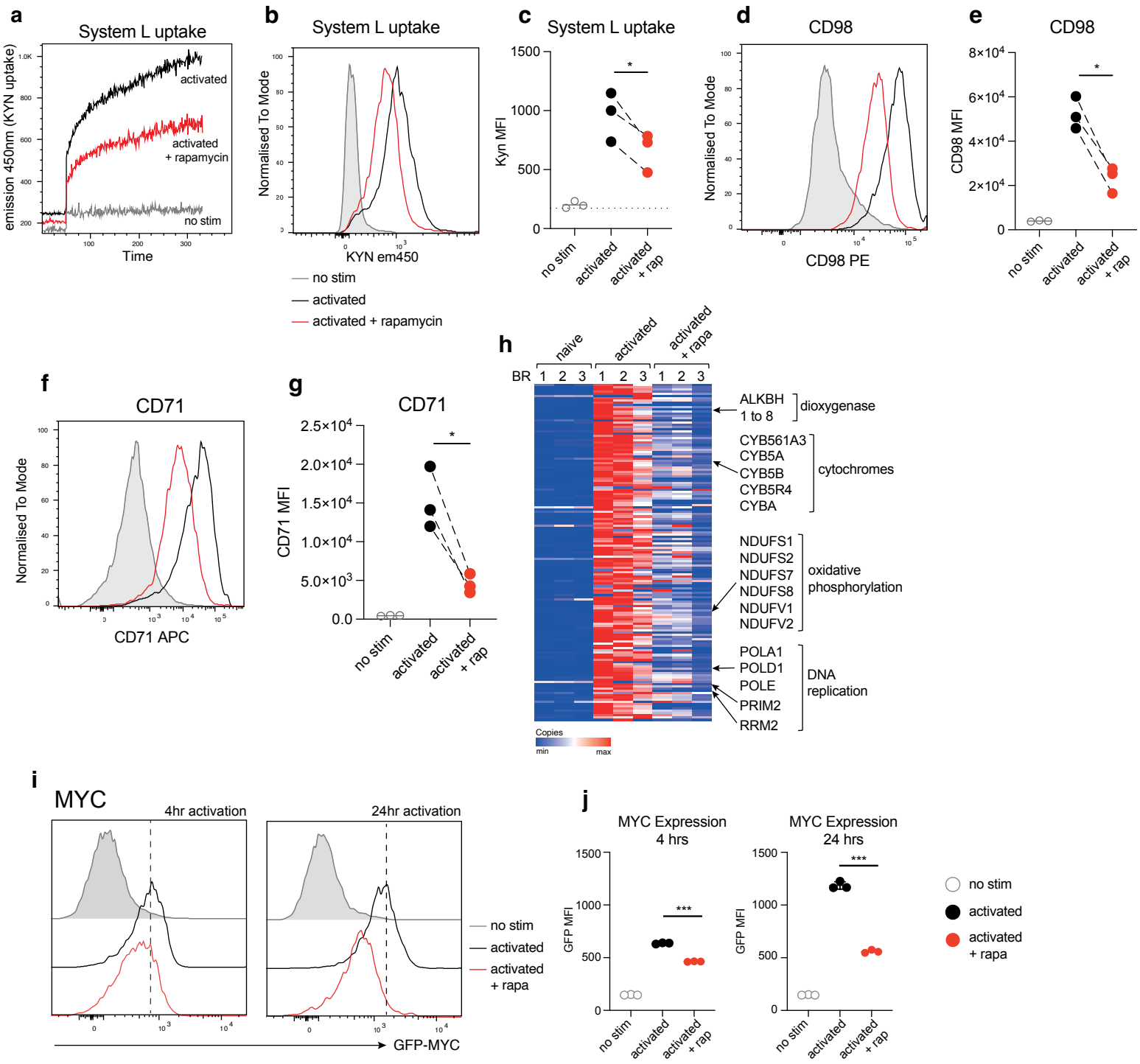
a
System L uptake
emission 450nm (KYN uptake)
activated
activated + rapamycin
no stim
Time
b
System L uptake
Normalised To Mode
KYN em450
no stim
activated
activated + rapamycin
c
System L uptake
Kyn MFI
no stim
activated
activated + rap
d
CD98
Normalised To Mode
CD98 PE
e
CD98
CD98 MFI
no stim
activated
activated + rap
f
CD71
Normalised To Mode
CD71 APC
g
CD71
CD71 MFI
no stim
activated
activated + rap
h
naive
activated
activated + rapa
BR 1 2 3 1 2 3 1 2 3
ALKBH 1 to 8
dioxygenase
CYB561A3
CYB5A
CYB5B
CYB5R4
CYBA
cytochromes
NDUFS1
NDUFS2
NDUFS7
NDUFS8
NDUFV1
NDUFV2
oxidative phosphorylation
POLA1
POLD1
POLE
PRIM2
RRM2
DNA replication
Copies
min
max
i
MYC
4hr activation
24hr activation
no stim
activated
activated + rapa
GFP-MYC
j
MYC Expression 4 hrs
MYC Expression 24 hrs
GFP MFI
no stim
activated
activated + rapa

Figure 6

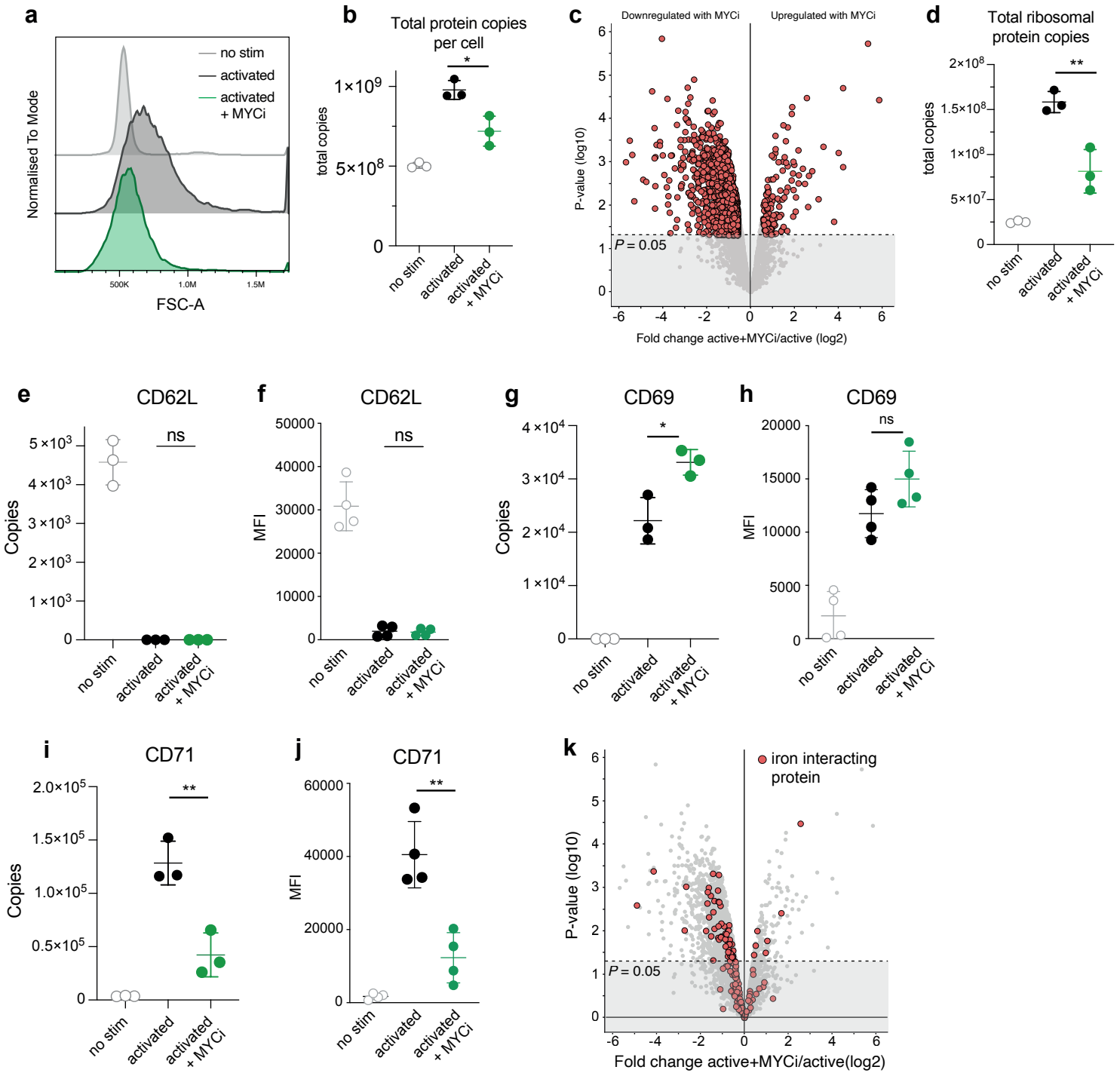
a
no stim
activated
activated + MYCi
Normalised To Mode
FSC-A
500K
1.0M
1.5M
b
Total protein copies per cell
total copies
1×10^9
5×10^8
0
*
no stim
activated
activated + MYCi
c
Downregulated with MYCi
Upregulated with MYCi
P-value (log10)
P = 0.05
Fold change active+MYCi/active (log2)
d
Total ribosomal protein copies
total copies
2×10^8
1.5×10^8
1×10^8
5×10^7
0
**
e
CD62L
Copies
ns
f
CD62L
MFI
ns
g
CD69
Copies
*
h
CD69
MFI
ns
i
CD71
Copies
**
j
CD71
MFI
**
k
iron interacting protein
P-value (log10)
P = 0.05
Fold change active+MYCi/active(log2)

Figure 7

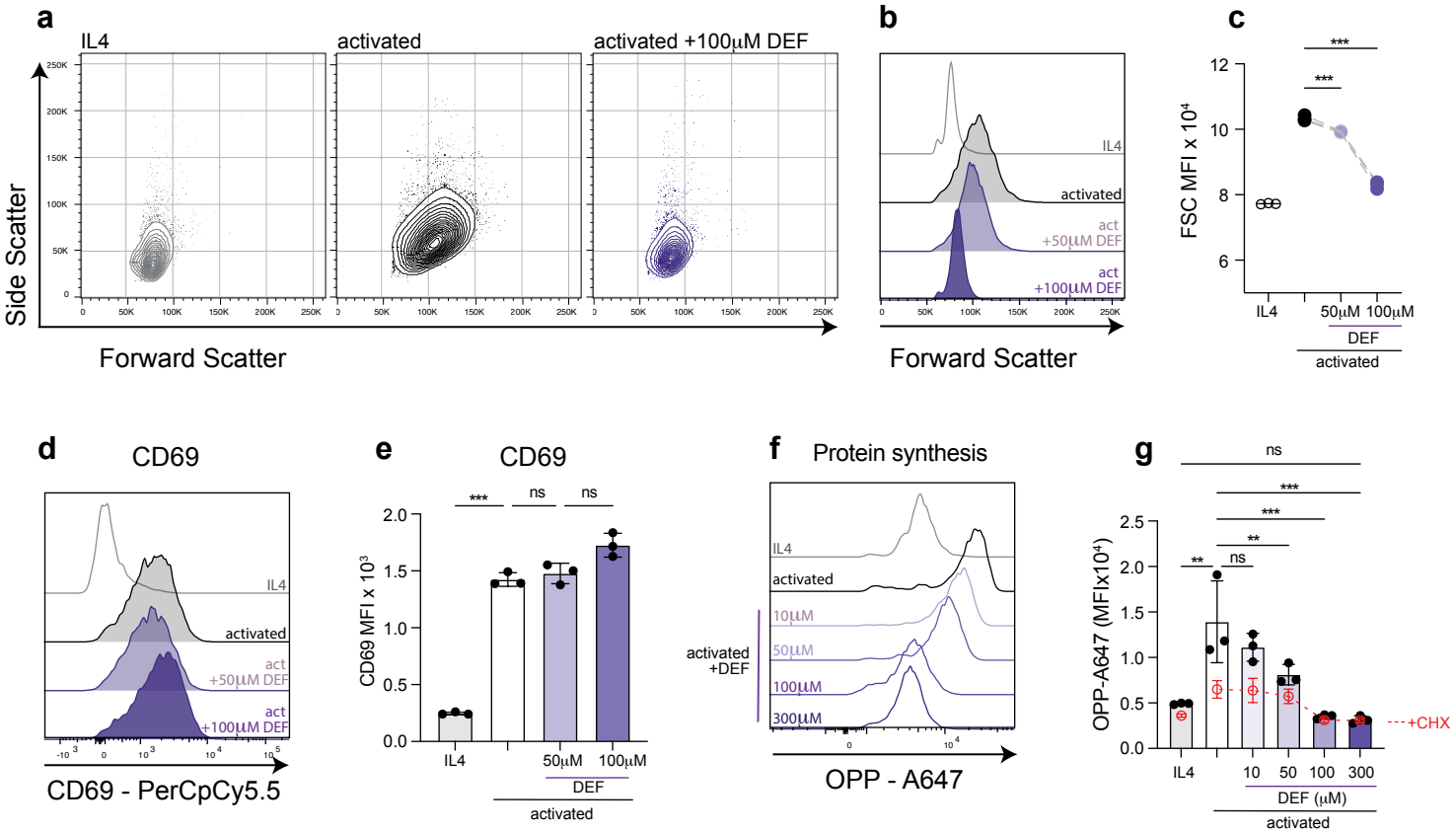
a
IL4
activated
activated +100µM DEF
Side Scatter
Forward Scatter
b
IL4
activated
act +50µM DEF
act +100µM DEF
Forward Scatter
c
FSC MFI x 10⁴
IL4
50µM
100µM
DEF
activated
d
CD69
IL4
activated
act +50µM DEF
act +100µM DEF
CD69 - PerCpCy5.5
e
CD69
CD69 MFI x 10³
ns
IL4
50µM
100µM
DEF
activated
f
Protein synthesis
IL4
activated
10µM
50µM
100µM
300µM
activated +DEF
OPP - A647
g
OPP-A647 (MFIx10⁴)
+CHX
IL4
10
50
100
300
DEF (µM)
activated